Combined single cell and single particle ICP-TQ-MS analysis to quantitatively evaluate the uptake and biotransformation of tellurium nanoparticles in bacteria

Beatriz Gomez-Gomez[1], Mario Corte-Rodríguez[2], Mª Teresa Perez-Corona[1], Jörg Bettmer[2], María Montes-Bayón[2], Yolanda Madrid[1,*]

[1] Complutense University of Madrid, Dept of Analytical Chemistry, Faculty of Chemistry. Avda. Complutense s/n 28040, Madrid. Spain

[2] University of Oviedo, Dept. of Physical and Analytical Chemistry and Instituto de Investigación Sanitaria del Principado de Asturias (ISPA), C/ Julián Clavería 8, E-33006 Oviedo, Spain.

*Corresponding Author:

Prof. Yolanda Madrid Albarran
Dept. of Analytical Chemistry
Faculty of Chemistry
Universidad Complutense de Madrid
E-28040 Madrid, Spain
Phone: +34913945145
Fax: +34913944329
e-mail: ymadrid@quim.ucm.es

Abstract

Assessing the impact of nanoparticles in living systems implies a proper evaluation of their behaviour at single-cell level. Due to the small size of nanoparticles, their accumulation, transformation and location within single cells is challenging. In this work, the combination of single cell/single particle triple quadrupole inductively coupled plasma mass spectrometry (SC/SP-ICP-TQ-MS) analysis along with X-ray diffraction (XRD) and transmission electron microscopy (TEM) measurements has been applied to go deeper into the uptake and biotransformation of tellurium nanoparticles (TeNPs) in two bacterial model organisms, *S. aureus* and *E. coli*. The use of SC-ICP-TQ-MS enabled the individual introduction of bacterial cells where tellurium and phosphorous (as constitutive element) were monitored and detected at concentration levels down to femtogram (fg) per cell. *S.aureus* uptake of TeNPs was 0.5-1.9 fg Te $cell^{-1}$ and 7-30 fg Te $cell^{-1}$ in presence of 0.5 and 15 mg Te L^{-1} of TeNPs, respectively, whereas for *E. coli*, the amount of Te ranged from 0.08 to 0.88 fg Te $cell^{-1}$ and from 2 to 36 fg Te $cell^{-1}$ in presence of 0.5 and 15 mg Te L^{-1} of TeNPs, respectively. TEM and XRD analysis confirmed the occurrence of TeNPs biotransformation (from nanospheres to nanorods) as the nanoparticles were incorporated into both bacterial strains. Finally, SP-ICP-MS analysis after cell lysis was applied to determine the number of particles/rods per bacteria cell and to perform the dimensional characterization of the rod-shaped TeNPs. The results obtained clearly confirmed high cell-to-cell variability in terms of Te nanorods dimensions and TeNPs uptake. To the best of our knowledge, this is the first time that SC/SP-ICP-TQ-MS along with TEM and XRD analysis have been applied to investigate, quantitatively, nanoparticle uptake in bacterial cells and to estimate the dimensions of biogenic Te nanorods.

Keywords: single cell ICP-MS; single particle ICP-MS; Tellurium nanoparticles; nanorods; *S. aureus*; *E. coli.*

1. Introduction

Application of metal/metalloid-based nanoparticles is increasing in areas directly related to our daily life. For example, nanoparticles are in the formulation of personal care and food products or textiles. Moreover, nanoparticles have attracted a great interest in medicine due to their potential as antimicrobial and drug delivery agents [1-5]. Unfortunately, the release of these nanomaterials into the environment is nowadays a matter of concern. Therefore, there is a need to elucidate the real impact of nanoparticles on ecosystems and human health, including a proper evaluation about their behaviour at single-cell level [6]. For this aim, there is also a limitation in the existing analytical tools. In fact, most of the reported studies on this topic estimate average contents of nanoparticle uptake in the entire cell population by performing classical bulk analysis of a large amount of cells after dissolution [7,8]. As a matter of fact, this approach does not provide information on cell to cell variability. Quantifying metal/metalloid based nanoparticles accumulation at single cell level is not an easy task due to both, the lack of appropriate methodologies and the difficulties found when performing cell lysis [9]. Moreover, this kind of studies becomes even more complicated when nanoparticles transformations in biological media take place [10].

Lately, ICP-MS-based analytical techniques for nanoparticles and cells determination such as single-particle ICP-MS (SP-ICP-MS) and single-cell ICP-MS (SC-ICP-MS), respectively, have emerged as powerful techniques for quantitatively assessing the impact of nanoparticles in living systems. SP-ICP-MS has been widely employed for sizing and quantifying nanoparticles in terms of number of nanoparticles in a wide range of matrices including consumer products, medical devices, biological tissues and environmental samples [11-15]. SC-ICP-MS follows a similar principle than SP-ICP-MS and is used to detect and quantify the metal content within individual cells [16]. In this approach, cells are directly nebulized (nowadays often using micro-flow nebulizers [17]) or micro-droplets dispensed into the plasma [18]. Then, the ions generated from

single cells are individually detected by applying high time resolution. In order to be successful in this type of analysis, it is crucial to obtain diluted cell suspensions and to introduce them into the plasma in the most efficient manner. For the latter purpose, special sample introduction systems are continuously being developed and improved by combining different micro-flow nebulizers with total consumption spray chambers [17,19, 20].

SC-ICP-MS has been successfully applied to evaluate the uptake of trace elements and metal-based nanoparticles by single human, algae or yeast cells [21-24]. However, its application to bacteria has been scarce, in spite of the fact that bacteria are crucial model organisms for assessing the impact of nanomaterials in the environment [25]. The main difference when performing analysis of human, algae, yeast or bacterial cells by SC-ICP-MS is the size of the different type of cells. Bacterial cells have a size smaller than algae, yeast or human cells. However, this aspect is not a problem; it could be actually an advantage. On the other hand, it is known that yeast cells are more resistant to mechanical disruption than bacterial cells. So, the main challenge found when analysing bacterial cells by SC-ICP-MS is to keep their physical integrity during their pass through the ICPMS system, from sample introduction system to the plasma. Although, this problem is inherent when analysing any type of cells by SC-ICP-MS it is even more accused when working with bacterial cells. The limited used of SC-ICP-MS for bacteria cells analysis could be also attributed to the novelty of the technique and consequently many of its applications are still under development.

In addition, most of the studies related to the quantification of nanoparticle uptake and distribution at single cell level have focused on well-known commercial nanoparticles such as silver or gold. Recently, tellurium-based nanoparticles (TeNPs) are being applied in various industrial fields such as the production of solar panels, glasses, new-generation rechargeable batteries and electronic devices as well as for environmental

remediation and biomedical applications [26-32]. However the knowledge about their impact on environment and living systems is quite limited

Although, the accuracy, precision and robustness of SP-ICP-MS have been clearly demonstrated, limitations arise when nanoparticles are far from having a spherical morphology, as calculations on their size distribution and concentration are based on the assumption that nanoparticles are spherical in shape. This limitation implies a serious problem when evaluating the behaviour of nanoparticles in living systems, as nanoparticles may undergo morphological changes when they are in contact with complex systems [33, 34].

Therefore, in this work we aim to study the fate and uptake of tellurium based nanoparticles (TeNPs) in two widely employed bacterial model organisms, *Staphylococcus aureus* and *Escherichia coli*, by combined single cell and single particle ICP-TQ-MS along with electron microscopy (TEM) and X-ray diffraction (XRD). The work has been divided into three parts: 1) nanoparticle characterization before and after being added to bacterial culture by TEM and XRD measurements in order to investigate morphological and compositional changes that nanoparticles may suffer as consequence of their interaction with bacteria, 2) quantification of accumulated TeNPs in individual bacterial cells at different exposure levels by performing SC-ICP-MS analysis, and 3) dimensional characterization of tellurium nanorods formed thorough the interaction of bacteria with the originally spherical TeNPs by employing TEM and SP-ICP-MS measurements. To the best of our knowledge, this is the first time that SC-ICP-MS and SP-ICP-MS along with TEM and XRD analysis have been applied to investigate nanoparticle uptake in bacterial cells and to estimate the dimensions of Tellurium nanorods.

2. Materials and Methods

2.1 Synthesis and characterization of tellurium nanoparticles (TeNPs)

Tellurium nanoparticles (TeNPs) were synthesized following the procedure previously reported by Gómez-Gómez et al. Briefly, the chemical reduction of potassium tellurite (K_2TeO_3, Sigma Aldrich) was carried out with gallic acid (Sigma Aldrich) in presence of hydroxyethyl cellulose (HEC, Sigma Aldrich) as coating agent [33,34]. After that, TeNPs were purified through a dialysis process. The characterization of these nanoparticles in terms of size, size distribution, morphology or composition, as well as their properties in solution (hydrodynamic diameter, the zeta potential and number particle concentration) has been already described in a previously published work [34]. Therefore, for this study, the nanoparticles synthesized were only submitted to a routine characterization before each experiment employing TEM (JEOL JEM 2100, Peabody, MA, USA) equipped with energy-dispersive X-ray spectroscopy (EDXS) microanalysis composition system (Oxford Instruments, High Wycombe, UK). Moreover, TeNPs were also characterized in the bacterial culture medium, Luria Bertani broth (LB), with the aim of assessing their stability under the same conditions as the subsequent studies.

On the other hand, Te nanorods found in bacterial cultures were also characterised by TEM. Image J software was used to obtain the values of width and length of the rod-shaped TeNPs from a representative amount of TEM images. In addition, X-ray diffraction pattern for rod-shaped TeNPs was obtained using a Panalytical X´PERT-MPD X-ray diffractometer (Malvern Panalytical, Ma, USA) operated at a voltage of 40 keV, 20 mA of current and 1.541 A of Cu Kα radiation.

2.2 Bacteria culture conditions and exposure to TeNPs

S. aureus (ATCC 29213) and *E. coli* (ATCC 25922) were cultured in Luria-Bertani (LB) medium and grown overnight at 37ºC under stirring (120 rpm). The obtained bacterial suspensions were diluted with LB solution until reaching an optical density (OD) of 0.1 at 620 nm. Then, bacterial cells were exposed to 0.5, 1 and 15 mg Te L^{-1} as TeNPs during 18h at 37ºC and 120 rpm. Non-incubated bacterial cells (control) were also treated in the same way. Three biological replicates were carried out for each experiment. Afterwards, bacterial cultures were centrifuged at 7000 rpm during 3 min. The supernatants were removed and the bacterial cell pellets were washed twice with Milli-Q water. Aliquots of 100 mg of bacterial pellet underwent an acid digestion with HNO_3/H_2O_2 (3:1). Finally, tellurium concentration in the digested pellet was measured by the triple quadrupole based Thermo iCAP TQ ICP-MS (Thermo Fisher Scientific, Bremen, Germany) using the single quadrupole mode. The ICP-MS was equipped with a Micro Mist nebulizer, a cyclonic spray chamber (both from Thermo Fisher Scientific) and an auto-sampler ASX-560 (Teledyne CETAC Technologies, Omaha, NE, USA). Furthermore, another aliquot from each bacterial culture was selected and monitored by TEM as described in the following section.

2.3 TeNPs internalization in bacteria by transmission electron microscopy (TEM)

Bacterial cells were exposed to different concentrations of TeNPs (as indicated above), then harvested by centrifugation at 7000 rpm during 3 min and finally washed with phosphate-buffered saline (PBS) (Sigma-Aldrich, St. Louis, MO, USA). Samples were then prepared for TEM observations through a process including fixation, dehydration, and embedding in a resin matrix. Briefly, bacterial cell pellets were fixed *in situ* with glutaraldehyde (2.5% v/v) (Sigma-Aldrich, St. Louis, MO, USA) and p-formaldehyde (4% v/v) (Sigma-Aldrich, St. Louis, MO, USA) in PBS at 4ºC for 4h. The resulting

mixture was subsequently treated with osmium tetraoxide (1% v/v) during 1h at room temperature under darkness and then dehydrated in graded acetone series (from 30% to 100 %). Afterwards, pellets were treated first with a mixture of resin:acetone, and finally, with 100% resin. The resulting blocks were incubated at 65ºC for 48h. Finally, ultrathin sections of samples were cut and examined by TEM.

2.4 Flow cytometry analysis

Flow cytometry measurements were performed in bacteria cell suspensions, in presence and absence of nanoparticles , to determine the percentage of viable and non-viable cells and to establish the number of bacterial cells with the aim of calculating the transport efficiency of the sample introduction system. For cytometry analysis, bacterial cultures exposed to TeNPs were washed three times with Tris-buffered saline (TBS, Sigma-Aldrich, St. Louis, MO, USA) solution and diluted with Milli-Q water until a bacterial cell concentration close to 10^5 cells mL^{-1} was achieved. After that, diluted bacterial cell suspensions were incubated with SYTO 9 and propidium iodide (PI) fluorescent dyes (Thermo Fisher Scientific, MA, USA) during 15 min. Finally, analyses were performed with a Flow Cytoflex S from Beckman Coulter (Brea, CA, USA).

2.5 Single cell analysis by ICP-TQ-MS

Bacterial cell suspensions obtained from the exposure experiments were washed three times with TBS and diluted with Milli-Q water to get a concentration in number of cells of approximately 10^5 cells mL^{-1}. Single-cell analysis was performed by using the iCAP TQ ICP-MS equipped with a high performance concentric nebulizer (HPCN) combined with the total consumption spray chamber (High Sensitivity Single-Cell Sample Introduction System for ICP-MS, Glass Expansion, Port Melbourne, Australia). Samples and rinsing solutions were introduced into the plasma at a flow rate of 10 µL min^{-1} using the MVX-7100 µL Workstation (Teledyne CETAC Technologies, Omaha,

NE, USA). Instrumental and data acquisition parameters are listed in Table S1. Measurements were carried out under time resolved analysis mode during 2 min per analysis with a dwell time of 5 ms and by selecting ^{126}Te as monitoring isotope. Furthermore, constitutive phosphorous chosen as constitutive cell element was measured as oxide ($^{31}P^{16}O^{+}$) in the triple quadrupole mode by using oxygen as reaction gas in a separate run. Transport efficiency of calibration standards was calculated by analysing citrate stabilized gold nanoparticle (AuNPs, nominal diameter 30 nm) standard (RM 8012) obtained from the NIST (Gaithersburg, MD, USA). Moreover, CyTOF Calibration Beads (Fluidigm Corporation, San Francisco, CA, USA) containing europium, at a particle number concentration of 33000 mL^{-1} (Fluidigm Corporation, San Francisco, CA, USA) were also employed to determine cell transport efficiency daily [35]. In order to performTe mass quantification by SP-ICP-MS analysis, a calibration curve of ionic tellurium was prepared daily within a concentration range from 0 to 50 µg L^{-1} with a tellurium standard for ICP obtained from Sigma Aldrich (St. Louis, MO, USA).

Data treatment of SC-ICP-MS analysis was carried out by applying an iterative procedure previously reported [19]. Briefly, the procedure consisted of selecting all data points that were three times the standard deviation (3σ) above the mean. The mean value was previously calculated by considering all the entire data set. The remaining data set was subjected again to the same procedure. The iterative procedure is repeated until there were no data points higher than the value of mean plus 3σ, and that value was used as threshold for cell events. Te amount in *S. aureus* and *E. coli* cells at a single-cell level was determined by applying Equation 1 [26]:

$$m_c = \frac{\eta \cdot F \cdot t \cdot I}{b} \qquad \text{(Equation 1)}$$

where m_c is the mass of the element in the cell, η is the transport efficiency for the liquid standards calculated using RM 8012 in the single particle mode, F is the sample

flow rate, t is the integration time, I is the count rate of Te, and b is the slope of the Te calibration curve previously measured.

Finally, to validate the data obtained from SC-ICP-TQ-MS analysis, the uptake of TeNPs by *S. aureus* and *E. coli* was assessed by means of ICP-TQ-MS (in single quad mode) after cell lysis, and referred to the number of bacteria present in the sample and counted by flow cytometry.

2.6 Bacteria cell disruption and single-particle ICP-MS (SP-ICP-MS) analysis of cell lysates

Bacterial cells were disrupted mechanically by using 0.5 mm glass beads (Merck Millipore, Darmstadt, Germany) and by adapting the procedure described by Álvarez-Fernández et al [23] . In this sense, 1 mL of bacterial cell suspensions was mixed with 734 mg of glass beads (500 µm of diameter) in an Eppendorf tube. Afterwards, the mixture was submitted to 5 min Vortex agitation followed by 10 min of sonication by means of an ultrasonic bath. The procedure was repeated twice for *E. coli*, but up to six cycles were needed to disrupt the *S. aureus* cells. Subsequently, cell debris and unbroken bacteria cells were removed appropriately by applying a centrifugation step at 2,000 g for 2 min. Particle mass quantification of TeNPs inside bacteria cells or adhered to bacterial membrane after bacterial cell disruption was performed by SP-ICP-MS and by applying the same procedure as for SC-ICP-TQ-MS analysis (described in section 2.5).

3. Results and Discussion

3.1 Accumulation and morphological transformation of TeNPs by *Staphylococcus aureus* and *Escherichia coli*.

The synthesis of the TeNPs resulted in the formation of spherical particles with a diameter of (125 ± 40) nm and with a composition of 80 % TeO_2 and 20 % Te. A

detailed characterization of the synthesized TeNPs is summarized in the Supporting Information (Figure S1).

The uptake of TeNPs by *S. aureus* and E. coli was assessed after their exposure to 0.5, 1 and 15 mg Te L-1 as TeNPs during 18h at 37ºC following the conditions described previously. Exposure levels were chosen based on previous studies published in the literature by the authors [33,34] who investigated the behaviour of TeNPs on bacterial biofilms developed by *S.aureus* and *E. coli*. In the current study the effect of TeNPs on *S. aureus* and *E. coli* was evaluated by selecting the same levels of TeNPs exposure as in previous studies but with the difference that bacterial cells were growth in planktonic mode.

The amount of Te accumulated was calculated by acid digestion of the bacterial pellet followed by ICP-TQ-MS analysis in single quad mode. The highest accumulation percentages were found for *S. aureus* reaching nearly 100 % for all levels of TeNPs administered, whereas the accumulation percentages in *E. coli* varied between 28% and 48% depending on the TeNPs concentration supplemented to the bacterial culture (Table 1).

Flow cytometry analyses were also performed in order to study the effect of TeNPs on *E. coli* and *S. aureus* viability. As shown in Table S2, around 80%-90% of bacterial cells were viable in case of *S. aureus* and *E. coli* regardless the amount of TeNPs supplemented.

It is important to notice that a change in the colour of the culture medium - from almost colourless to deep black - was observed when the highest concentration of TeNPs was supplemented to both bacterial strains. In contrast, no variation in the culture medium colour was observed when TeNPs were dispersed in LB medium in absence of bacteria. The observed colour changes were associated with the appearance of tellurium nanorods as shown in Figures 1a and b. The presence of tellurium nanorods

was only detected in presence of high particle concentration of 15 mg L^{-1}, but not at 0.5 and 1 mg Te L^{-1} levels. This fact can be explained as 0.5 and 1 mg Te L^{-1} were very low Te levels to be observed by TEM. The electron diffraction pattern composed by concentric rings presented in TEM images (Figures 1a and b) confirmed the crystalline structure of the rod-shape tellurium nanoparticles. The morphological change observed (from spherical to nanorod shape) can be linked to a detoxification mechanism as it has been also reported for SeNPs and TeNPs in different bacteria strains, suggesting a low toxicity against bacteria of rod-shape nanoparticles compared to spherical ones [36-40]. To the best of our knowledge, the morphological transformation of TeNPs from spheres to nanorods after being exposed to *S. aureus* and *E. coli* planktonic cells has not been reported to date.

Size of tellurium nanorods was determined by counting more than 200 individual particles from different TEM images and by employing the Image J software. It was found that the length and width of Te nanorods in *E. coli* experiments were (303 ± 23) nm and (26 ± 10) nm, respectively, with an aspect ratio of around 12. The respective data for *S. aureus* were (267 ± 129) nm and (21 ± 8) nm with an aspect ratio of around 14. Additionally, the phase and composition of tellurium nanorods were also determined by X-ray diffraction. Figures 1c and 1d display XRD spectra obtained from *S. aureus* and *E. coli* treated with TeNPs. In the case of *S. aureus*, peaks of tellurium nanorods were indexed as cubic phase (Fd-3m space group: 227) and rhombohedral phase (R-3m space group: 166) of Te crystal and as orthorombic phase of crystalline TeO_2 (Pnma space group: 62). These values agreed well with the standard literature data (card number 04-002-3701, 04-015-6838 and 04-022-7519 respectively). Moreover, XRD analysis indicated that tellurium nanorods were composed of 99% $Te0_2$ and 1% Te. With respect to *E.coli,* peaks of tellurium nanorods were assigned to cubic phase (Fd-3m space group: 227) and monoclinic phase (P21 space group: 4) of Te crystal and orthorombic phase of TeO_2 (Pnma space group: 62) which is in good

agreement with the standard literature data (card number 04-002-3701, 04-007-2056 and 04-022-7519 respectively). XRD measurements indicated that tellurium nanorods were also composed of 99% TeO_2 and 1% Te.

The results obtained clearly demonstrate important morphological and compositional changes in nanoparticles as they interact with bacterial cells. Nanoparticle adhesion to bacteria cell surface or internalization into bacteria cells are two of the most plausible mechanisms that may happen as consequence of the bacterial exposure to nanoparticles interaction. TEM images from Figures 1a and b have evidenced that TeNPs interact with bacteria surface. Unfortunately, TEM images were not clear enough to ensure whether nanoparticles were inside of bacteria cell or just attached to bacterial membranes. To correctly locate nanoparticles in relation to bacterial cells, TEM images of chemically fixed bacteria cells (by applying the procedure described previously) were acquired to corroborate the information gathered from TEM images previously described (Figure 1a and b). Figure 2 shows sectioned TEM images of *E. coli* and *S. aureus* in presence of 0, 1 and 15 mg Te L^{-1} as TeNPs. In *E. coli* experiments, it is difficult to ensure the presence of nanoparticles inside the bacteria at 1 mg Te L^{-1} as TeNPs, due to the fact that the concentration of tellurium was too low to be detected by TEM microscopy (Figure 2b). However, bacterial cell surface damage can be clearly detected (Figure 2b) in comparison to the control cells (Figure 2a). Concerning to *E. coli* treated with 15 mg Te L^{-1}, tellurium nanorods can be found (highlighted with white arrows) either on the surface of the bacterial cell wall or inside the bacterial cell, probably in the cytoplasm (Figures 2c and d). Morphological changes in bacteria cell surface along with vesicles and ruffled extensions of the bacterial plasma membrane (red arrows) are detected. Endocytosis has been described as one of the most likely mechanism of nanoparticles internalization into cells [41]. Sectioned TEM images of *E. coli and S. aureus* treated with the lowest level of TeNPs (0.5 mg Te L^{-1} as TeNPs) are depicted in Figure S2 of the Supporting Information.

Similarly, in the case of *S. aureus*, no particles attached to the bacteria membrane or inside the bacteria were observed at 1 mg Te L^{-1} as TeNPs (Figure 2f). After incubation with 15 mg Te L^{-1} as TeNPs (Figure 2g) rod-shaped tellurium nanoparticles (white arrows) were present either associated to bacteria membrane or inside bacterial cells. Once again, vesicles as consequence of an endocytosis process were perceived (red arrows, Figure 2h). In addition, nanoparticles might induce other membrane deformation and lysis as well as a release of cytoplasmic contents (yellow arrows, Figures 2g and h).

3.2 Quantitative analysis of TeNPs uptake at single cell level.

Up to this point, the uptake and accumulation of TeNPs in *S. aureus* and *E. coli* was measured and averaged within the entire cell population and assuming that all bacterial cells incorporate the same number of nanoparticles. However, it is well known that metals and nanoparticles are heterogeneously distributed in cells. Single-cell ICP-MS has been employed in this work to perform TeNPs uptake profiling at single bacterial cell level. The analytical determination of TeNPs by SC-ICP-MS is challenging since the information about these nanoparticles (physicochemical properties, behaviour in living systems such as cell and bacteria) is really scarce compared to other better characterized as AuNPs and AgNPs [21,24].

For performing SC-ICP-MS analysis, a high performance concentric nebulizer with a total consumption spray chamber was employed. This combination enabled the introduction of intact bacteria into the plasma with a transport efficiency as high as 60 %. No statistically significant differences of transport efficiencies were found either for AuNPs (NIST 8012) or for 2.5 µm polystyrene CyTOF calibration beads loaded with europium as standard suspensions. To ensure that each individual ICP-MS signal corresponds to a single cell, the cell density was adjusted to approximately around 10^5 cells per mL.

Moreover, the efficiency of the cell introduction system was calculated by comparing data from the bacterial cell population, counted by flow cytometry, and the number of cell signals obtained for the constitutive element phosphorus (monitored as $^{31}P^{16}O^{+}$) in the single cell ICP-MS experiments [23]. Under optimal experimental conditions, the cell introduction efficiency was (74 ± 6) % and (85 ± 7) % for *E. coli* and *S. aureus*, respectively. Differences in the percentages of the introduction efficiency might be attributed to differences in bacterial cell size, 2.14±0.52 µm for *E.coli* and 0.74±0.12 µm for *S.aureus* (according to data from TEM micrographs).

The amount of TeNPs (expressed as Te) at single-cell level was calculated by using an external calibration curve obtained with a tellurium standard solution followed by data processing as described in the experimental section. The limit of detection (LOD) was found to be (0.068 ± 0.008) fg Te per cell. Figures 3a-d and 4a-d show time-resolved analyses of $^{126}Te^{+}$ obtained from *S. aureus* and *E. coli* cultures, respectively, after being exposed to TeNPs.

As shown in Figures S3 and S4, the number of phosphorus events decreased with increasing TeNPs concentrations from 2031 to 1503 for *S. aureus* and from 3643 to 427 for *E. coli*. The results show the influence of TeNPs on cell population density being more pronounced in the case of E. coli. On the contrary, a significant number of events, with increasing intensities of $^{126}Te^{+}$ as TeNPs concentration raised, could be observed in Figures 3b-d and 4b-d, whereas no spike signals were detected in the control samples (Figures 3a and 4a). Therefore, those spike signals that fulfil the criterion of being three times higher than the mean value of the background baseline were gathered and transformed into Te mass (fg) per single cell. Mass distribution histograms showing Te mass per individual cell (fg Te per cell) at each supplemented TeNPs concentration are displayed in Figures 3e-g and 4e-g for the two bacterial strains. As it was previously indicated, a LOD value of 0.068 fg Te per cell was obtained in this study which means that we were able to detect levels of Te

accumulated higher than the LOD, such as 0.5, 0.6 or 7 fg Te per cell as shown in in Figures 3g, e and f. We did not detect any concentration below 0,5 fg per cell as the bacterial cells accumulated greater amount of Te than 0.5fg/cell. Similarly, accumulation values much higher than LOD were determined for *E coli* and ranged from 0.8 to 2 fg Te per cell as shown in the frequency histograms depicted in figure 4g, e and f.

As it was expected, the mass of TeNPs accumulated in individual bacteria is heterogeneously distributed for each experimental condition tested. Moreover, results from SC-ICP-TQ-MS analysis in single quad mode confirmed that TeNPs were either internalized or adsorbed onto the bacterial cell wall even at low levels of exposure such as 0.5 and 1 mg Te L-1 as TeNPs. As it was previously mentioned, TEM was not able to visualize the accumulation of TeNPs in bacteria population at these low TeNPs levels of exposure. The average amount of Te per cell varied from (0.77 ± 0.22) fg per cell to (12.80 ± 5.58) fg cell for *S. aureus* and (0.30 ± 0.13) fg per cell to (12.43 ± 4.36) fg per cell for *E. coli* (Table 2).

The percentage of *E. coli* cells containing Te increased from 35% to 59% for bacterial cells exposed to 0.5 and 1 mg Te L^{-1} up to 94% at the highest level of exposure. In the case of *S. aureus*, the percentages increased from 57% to 76% for cells exposed to the lower concentrations up to 100 % at 15 mg Te L^{-1}. ANOVA analysis evidenced statistically significant differences ($P<0.05$) among values for Te amount per cell for those bacteria treated with 0.5 and 1 mg Te L^{-1} compared to 15 mg Te L^{-1} as well as statistically significant differences between the Te amount found in both strains and in the presence of 0.5 and 0.1 mg Te L^{-1} as TeNPs (Table 2). It is important to notice that data in Table 2 is referred only to bacterial cells that accumulate TeNPs. Bacteria cells that did not accumulate TeNPs were not detected by SC-ICP-MS since Te signal was monitored. The total bacterial cell population was estimated by monitoring the phosphorus signal in SC-ICP-MS measurements.

The accuracy of the data provided by SC-ICP-TQ-MS for quantifying Te at individual bacterial cell level was thereafter assessed by combining ICP-TQ-MS in single quad mode after acid digestion (total Te concentration per bacterial cell) and flow cytometry (total bacterial cell population) measurements. As shown in Table 2, there is a good agreement between results obtained by both methods. Consequently, SC-ICP-TQ-MS seems to provide accurate data about the mass of TeNPs uptaken by individual bacterial cells with the advantage of delivering information on the variability from cell to cell

3.3 Determination of the number of TeNPs per individual bacterial cells.

The number of individual particles either internalized or adhered to bacteria wall was determined after the mechanical bacterial cell lysis with glass beads. The performance of the method applied for bacterial cell disruption was assessed by monitoring the signals of phosphorous before and after applying the lysis procedure. Around a (90 ± 4) % and (92 ± 2) % of the cells were disrupted in S. aureus and E. coli experiments, respectively. Furthermore, tellurium was also monitored in a second run. The time resolved analyses for Te in Figure 5 demonstrates that the intensity of the events decreased after applying cell disruption at 15 mg Te L.1. Although this effect was detected for all levels of exposure, it was more pronounced at 15 mg Te L-1 as TeNPs. The results obtained may corroborate that TeNPs were internalized by the bacterial cells or attached to bacteria cell wall.

After the disruption of the cell walls, the intensity of the events produced by individual nanoparticles was lower than those related to intact cells that could have accumulated more than one TeNP. With the knowledge of the mass of an individual particle and the mass of Te accumulated per cell from previous sections, the number of TeNPs internalized or associated to bacterial cell wall was calculated. Table 3 displays the average of nanoparticles detected in individual bacterial cells as well as the minimum and maximum number of particles after exposure to the three different Te

concentrations. The number of particles increased with the applied TeNPs concentrations. Cells containing one single TeNP only appear at 0.5 mg Te L-1 whereas cells containing multiple TeNPs were detected at the higher concentrations in both bacterial strains.

No significant differences between strains regarding to the number of particles accumulated were observed, although the maximum number of particles was higher in E. coli, probably due to the increased cell size.

3.4 Sizing rod-shaped TeNPs by SP-ICP-MS and TEM measurements

Finally, the dimensional characterization of tellurium nanorods formed through the interaction of bacteria with the original spherical TeNPs was explored. Single-particle ICP-MS is a valuable technique that enables the mass determination of individual particles. Provided that the particles are of spherical shape, it is well established to convert the mass of the particle into its size [42]. However, characterization of non-spherical nanoparticles by employing SP-ICP-MS is still in its infancy [43].

In the current work, dimensional size characterization of rod-shaped tellurium nanoparticles has been performed by employing TEM and SP-ICP-MS analysis. It is important to highlight that the calculations for estimating the width and length of tellurium nanorods have been carried out by considering these nanoparticles with a cylindrical morphology. The procedure developed consisted on a step-by-step approach: 1) determination of the volume of nanorods by particle mass data (SP-ICP-TQ-MS) and particle density (from nanorods composition provided by X-ray diffraction, considering 99 % TeO_2 and 1 % Te) and 2) estimation of width and length of tellurium nanorods by employing the formula for the volume of a cylinder and the aspect ratio previously determined by TEM analysis. The particle size detection limit for SP-ICP-MS was calculated by using the approach of Abad-Alvaro et al [44] and by applying the 3σ criterion. Based on that , the LOD size was 28 nm. Therefore, those particles with a

volume below 11,494 nm3 were not considered for tellurium nanorods dimensional estimations. Consequently, and by assuming a LOD size of 28 nm, the smallest volumes employed for calculations were about 12,505 nm^3 and 15,492 nm^3 for *E. coli* and *S. aureus* experiments, respectively and corresponding to a minimum width of around 11 and 12 nm. A similar procedure has been reported by Kalomista *et al.* for dimensional size characterization of rod-shaped gold nanoparticles [43].

Figures 6 and 7 show width and length size histograms calculated from tellurium nanorods isolated from *E. coli and S. aureus*, respectively, after exposure to the different Te concentrations. The histogram profiles clearly demonstrate the variability of the nanorods dimensions, which confirms the heterogeneity of bacterial cell behaviour concerning the morphological TeNPs transformations and uptake. Furthermore, mean values for width and length calculated with SP-ICP-MS agreed well with those values provided by TEM at the highest concentration of TeNPs tested. No TEM data were available for comparison at the low exposition levels, since this technique was unable to detect the nanorods under those conditions. However, the SP-ICP-MS strategy developed here, is capable of providing data on the size of the nanorods at the lowest levels of exposure (0.5 and 1 mg Te L^{-1}), confirming that these are similar in width, but shorter in length than the ones produced after exposure to 15 mg Te L^{-1} in both species of bacteria.

4. Conclusions

This study shows for the first time the application of SC-ICP-TQ-MS for quantifying the uptake and distribution of TeNPs at single cell level in Gram-positive and Gram-negative bacteria model organisms, *S. aureus* and *E. coli*, respectively. Moreover, the combination of flow cytometry (bacterial cell population) and ICP-TQ-MS (phosphorous content) has enable to track cell transport until the plasma, achieving under optimal conditions, cell introduction efficiencies as high as (74 ± 6) % and (85 ± 7) % for *E. coli* and *S. aureus*, respectively. The results obtained confirmed the existence of a great

cell to cell variability in terms of TeNPs uptake and number of particles accumulated. TEM analysis together with X-ray diffraction measurements evidenced compositional and morphological changes of TeNPs from nanospheres to nanorods as a consequence of bacteria-nanoparticle interaction. The combination of SP-ICP-MS and TEM has allowed us to estimate the dimensions of nanorods produced by both bacterial strains. The values obtained agreed well with the values calculated from TEM images confirming the feasibility of the proposed strategy for the dimensional characterization of non-spherical nanoparticles and overcoming size limitations for TEM detection.

Author contributions

All authors have given approval to the final version of the manuscript.

Notes

The authors declare no competing financial interest.

Acknowledgements

The authors gratefully acknowledge the financial support from Spanish Ministry for Science, Innovation and Universities (CTQ2017-83569-C2-1-R, RTI2018-094605-B-I00, FC-GRUPIN-IDI/2018/000242), the Community of Madrid and European funding from FSE and FEDER programs (project S2018/BAA-4393, AVANSECAL-II CM), as well as the support from the Asturian Foundation for Biosanitary Research and Innovation (FINBA). Thermo Fisher Scientific, Bremen, Germany, and Teledyne Cetac Technologies, Omaha, NE, USA, are acknowledged for their instrumental support.

Supporting Information.

Table S1: Operating parameters of the ICP-TQ-MS system for the single cell and single cell experiments. Table S2: Percentage of viable and non-viable cell after the exposure of *S.aureus* and *E.coli* to TeNPs obtained from flow cytometry analysis (mean ± SD; n=3). Figure S1:TEM images and EDXS spectrum of TeNPs dispersed

(a) in water and (b) in LB medium. (c) X-ray diffraction pattern of TeNPs. Figure S2: TEM images of a thin section of fixed E. coli (a) and S.aureus (b) treated with (0.5 mg Te L^{-1} as TeNPs. Figure S3:Time resolved SC-ICP-MS analysis of $^{31}P^{16}O+$ for S. aureus cells treated with (a) 0, (b) 0.5, (c) 1, and (d) 15 mg Te L-1 as TeNPs. Figure S4. Time resolve SC-ICP-MS analysis of ^{31} P16O+ for E, coli treated with with (a) 0, (b) 0.5, (c) 1, and (d) 15 mg Te L-1 as TeNPs.

Figures Captions

Figure 1: TEM images, EDXS spectra and concentring ring (a, b) and X-ray diffraction pattern (c, d) of rod-shaped TeNPs found in (a, c) *S. aureus* and (b, d) *E. coli* experiments.

Figure 2: TEM images of a thin section of fixed E. coli treated with (a) 0, (b) 1, and (c and d) 15 mg Te L^{-1} as TeNPs and *S. aureus treated* with (e) 0, (f) 1.0, and (g and h) 15 mg Te L^{-1} as TeNPs. Red arrows indicate morphological changes in bacteria and white arrows rod-shaped TeNPs.

Figure 3: Time resolved SC-ICP-MS analyses of (a-d) ^{126}Te and the corresponding frequency histograms (e-g) for *S. aureus* cells treated with (a) 0, (b) 0.5, (c) 1, and (d) 15 mg Te L^{-1} as TeNPs.

Figure 4: Time resolved SC-ICP-MS analyses of (a-d) ^{126}Te and the corresponding frequency histograms (e-g) for *E. coli* cells treated with (a) 0, (b) 0.5, (c) 1, and (d) 15 mg Te L^{-1} as TeNPs.

Figure 5: Time resolved SC/SP-ICP-MS analyses of ^{126}Te before (a and c) and after bacterial wall disruption (b and d) of *E. coli* (a and b) and *S. aureus* (c and d) cells treated with 15 mg Te L^{-1} as TeNPs.

Figure 6: Size distribution histogram obtained from SP-ICP-MS analysis for width and length dimensions of rod-shaped TeNPs isolated from *E. coli* cells treated with (a and b) 0.5, (c and d) 1 and (e and f) 15 mg Te L^{-1} as TeNPs.

Figure 7: Size distribution histogram obtained from SP-ICP-MS analysis for width and length dimensions of rod-shaped TeNPs isolated from *S. aureus* cells treated with (a and b) 0.5, (c and d) 1 and (e and f) 15 mg Te L^{-1} as TeNPs.

Tables.

Table 1: Percentage of Te accumulated in *S.aureus* and *E. coli* after their exposure to different concentration of TeNPs (mean ± SD; n=3).

	S.aureus	*E.coli*
[TeNPs] mg Te L^{-1}	% Te	% Te
0.5	97 ± 3	48 ± 3
1	100 ± 10	38 ± 1
15	105 ± 9	28 ± 4

Table 2: Te levels in *S. aureus* and *E .coli* after incubation with 0.5, 1, 15 mg Te L^{-1} as TeNPs by SC-ICP-MS and after acid digestion (mean ± SD; n=3).

	S. aureus		*E. coli*	
[TeNPs] mg Te L^{-1}	SC-ICP-MS fg cell $^{-1}$	Digestion /ICP-MS fg cell $^{-1}$	SC-ICP-MS fg cell $^{-1}$	Digestion /ICP-MS fg cell^{-1}
0.5	0.77 ± 0.22	0.79 ± 0.12	0.30 ± 0.13	0.24 ± 0.10
1	1.20 ± 0.53	1.10 ± 0.22	0.44 ± 0.21	0.47 ± 0.21
15	12.80 ± 5.58	18.19 ± 2.34	12.43 ± 4.36	14.96 ± 2.52

Table 3: Average of TeNPs internalized or associated to bacteria cell wall per *S. aureus* and *E. coli* individual cell after the incubation of both strains with 0.5, 1, 15 mg Te L^{-1} as TeNPs determined by SP-ICP-MS after bacterial cell lysis.

[TeNPs]	*S.aureus*			*E.coli*		
mg Te L^{-1}	TeNPs $cell^{-1}$			TeNPs $cell^{-1}$		
	Min	Max	Mean	Min	Max	Mean
0.5	1	9	5 ± 2	1	4	4 ± 1
1	2	13	9 ± 4	2	11	7 ± 3
15	3	95	37 ± 27	3	122	50 ± 36

References

[1] Nasrollahzadeh, M.; Sajadi, S.M.; Sajjadi, M.; Issaabadi, Z. Application of nanotechnology in daily life. *Interf. Sci. Technol.* **2019**, 28, 113-143.

[2] Katz, L.M.; Dewan, K.; Bronaugh, R.L. Nanotechnology in cosmetics. *Food Chem. Toxicol .* **2015**, 85, 127- 137.

[3] Gupta, R.; Xie, H. Nanoparticles in daily life: Applications, Toxicity and Regulations. *J. Environ. Pathol. Toxicol. Oncol.* **2018**, 37(3), 209-230.

[4] Pathakoti, K.; Manubolu, M.; Hwang, H.M. Nanostructures current uses and future applications in food science. *J. Food Drug Anal.* **2017**, 25, 245-253.

[5] Zheng, K.; Setyawati, M.I.; Leong, F.T.; Xie, J. Antimicrobial silver nanomaterials. *Coord. Chem. Rev.* **2018**, 357, 1-17.

[6] Lead, J.R.; Batley, G.E.; Alvarez, P.J.J.; Croteau, M.N.; Handy, R.D.; McLaughlin, M.J.; Judy, J.D.; Schrimer, K. Nanomaterials in the environment: behavior, fate, bioavailability, and effects-an updated review. *Environ. Toxicol. Chem.* **2018**, 37, 2029-2063.

[7] Kruszewska, J.; Kur, A., Kulpinska, D.; Grabowska-Jadach, I.; Matczuk, M.; Keppler, B.K.; Timerbaev, A.R.; Jarosz, M. An improved protocol for ICP-MS based assessment of the celular uptake of metal-based nanoparticles. *J. Pharm. Biomed. Anal.* **2019**, 174, 300-304.

[8] Matczuk, M.; Ruzik, L.; Alksenko, S.S.; Keppler, B.K.; Jarosz, M.; Timerbaev, A.R. Analytical methodology for studying cellular uptake, processing and localization of gold nanoparticles. *Anal. Chim. Acta* **2019**, 1052, 1-9.

[9] Wei, X.; Dong-Hua, Z.; Cai, Y.; Jiang, R.; Chen, M.L.; Yang, T.; Xu, Z.R.; Yu, Y.L.; Wang, J.H. High-Throughput/High-Precision sampling of single cells into ICP-MS for elucidating cellular nanoparticles. *Anal. Chem.* **2018**, 90, 14543-14550.

[10] Merrifield, R. C.; Stephan, C.; Lead, J. Determining the concentration dependent transformations of Ag nanoparticles in complex media: Using SP-ICP-MS and Au@Ag core shell nanoparticles as tracers. *Environ. Sci. Technol.* **2017**, 51, 3206−3213.

[11] Loeschner, K.; Navratilova, J.; Kobler, C.; Molhave, K.; Wagner, S.; von der Kammer, F.; Larsen, E.H. Detection and characterization of silver nanoparticles in chicken meat by asymmetric flow field flow fractionation with Detection by conventional or single particle ICP-MS. *Anal. Bioanal. Chem.* **2013**, 405, 8185-8195.

[12] Loeschner, K.; Brabrand, M.S.J.; Sloth, J.J.; Larsen, E.H. Use of alkaline or enzymatic sample pretreatment prior to characterization of gold nanoparticles in animal tissue by single-particle ICPMS. *Anal. Bioanal. Chem.* **2014**, 406, 3845-3851.

[13] Peters, R.J.; Rivera, Z.H.; Van Bemmel, G.; Marvin, H.J.; Weigel, S.; Bouwmeester, H. Development and validation of single particle ICP-MS for sizing and quantitative determination of nano-silver in chicken meat. *Anal. Bioanal. Chem.* **2014**, 406, 3875-3885.

[14] Dan, Y.; Zhang, W.; Xue, R.; Ma, X.; Stephan, C.; Shi, H. Characterization of gold nanoparticle uptake by tomato plants using enzymatic extraction followed by single-particle inductively coupled plasma-mass spectrometry analysis. *Environ. Sci. Technol.* **2015**, 49, 3007-3014.

[15] Laborda, F.; Bolea, E.; Jimenez-Lamana, J. Single particle inductively coupled plasma mass spectrometry for the analysis of inorganic engineered nanoparticles in environmental samples. *Trends Environ. Anal. Chem.* **2016**, 9, 15-23.

[16] Li, F.; Armstrong, D. W.; Houk, R. S. Behavior of bacteria in the inductively coupled plasma: Atomization and production of atomic ions for mass spectrometry. *Anal. Chem.* **2005**, 77, 1407-1413.

[17] Wang, H.; Wang, M.; Wang, B.; Zheng, L.; Chen, H.; Chai, Z.; Feng, W. Interrogating the variation of element masses and distribution patterns in single cells using ICP-MS with a high efficiency cell introduction system. *Anal. Bioanal. Chem.* **2017**, 409, 1415-1423.

[18] Shigeta, K.; Koellensperger, G.; Rampler, E.; Traub, H.; Rottmann, L.; Panne, U.; Okinoc, A.; Jakubowski, N. Sample introduction of single selenized yeast cells (Saccharomyces cerevisiae) by micro droplet generation into an ICP-sector field mass spectrometer for label-free detection of trace elements. *J. Anal. At. Spectrom.* **2013**, 28:637-645.

[19] Corte, M.; Alvarez-Fernández, R.; Blanco, E.; Bettmer, J.; Montes-Bayón, M. Quantitative evaluation of cisplatin uptake in sensitive and resistant individual cells by single-cell ICP- MS (SC-ICP-MS). *Anal. Chem.* **2017**, 89, 11491-11497.

[20] Wang, H.; Chen, B.; He, M.; Hu, B. A facile Droplet-Chip-Time-Resolved Inductivvely Coupled Plasma Mass Spectrometry Online System for determination of zinc in single cell. *Anal. Chem.* **2017**, 89(9), 4931-938

[21] Lopez-Serrano, A.; Baumgart, S.; Bremser, W.; Fleming, S.; Wittke, D.; Grützkau, A.; Luch, A.; Haase, A.; Jaubowski, N. Quantification of silver nanoparticles up-taken by single cell using inductively coupled plasma mass spectrometry in the single cell measurement mode. *J. Anal. At. Spectrom.* **2018**, 33, 1256-1263.

[22] Mavrakis, E.; Mavroudakis, L.; Lydakis-Simantiris, N.; Pergantis, SA. Investigating the uptake of arsenate by Chlamydomonas reinhardtii cells and its effect of their lipid profile using single cell ICP-MS and easy ambient sonic-spray ionization-MS. *Anal. Chem.* **2019**, 91, 9590-9598.

[23] Álvarez-Fernández García, R.; Corte-Rodríguez, M.; Macke, M.; LeBlanc, K.; Mester, Z.; Montes-Bayon, M.; Bettmer, J. Addressing the Presence of Biogenic Selenium Nanoparticles in Yeast Cells: Analytical Strategies Based on ICP-TQ-MS. *Analyst* **2020**, DOI: 10.1039/C9AN01565E.

[24] Merrifield, R.C.; Stephan, C.; Lead, J.R. Quantification of Au nanoparticles biouptake and distribution to freshwater algae using single cell ICP-MS. *Environ. Sci. Technol.* **2018**, 52, 2271-2277.

[25] Feng, Z.V.; Gunsolus, I.L.; Qiu, T.A.; Hurley, K.R.; Nyberg, L.H.; Frew, H.; Johnson, K.P.; Varanian, A.; Jacob, L.M.; Lohset, S.E.; Torelli, M.D.; Hamers, R.J.;

Murphy, C.J.; Haynes, C.L. Impact of gold nanoparticle charge and ligand type on surface binding and toxicity to Gram-negative and Gram-positive bacteria. *Chem. Sci.* **2015**, 6, 5186-5196.

[26] Nguyen, V.K.; Choi, W.; Ha, Y.; Gu, Y.; Lee, C.; Park, J.; Jang, G.; Shin, C.; Cho, S. Microbial tellurite reduction and production of elemental tellurium nanoparticles by novel bacteria isolated from wastewater. *J. Ind. Eng. Chem.* **2019**, 78, 246-256.

[27] Mousavi-Kamazani, M.; Rahmatolahzadeh, R.; Shobeiri, S.A.; Beshkar, F. Sonochemical synthesis, formation mechanism, and solar cell application of tellurium nanoparticles. *Ultrason. Sonochem*. **2017**, 39, 233-239.

[28] Ba, L.A.; Doring, M.; Jamier, V.; Jacob, C. Tellurium: an element with great biological potency and potential. *Org. Biomol. Chem*., **2012**, 8(19), 4203-16.

[29] Figueroa, M.; Fernandez, V.; Arenas-Salinas, M.; Ahumada, D.; Muñoz-Villagrán, C.; Cornejo, F.; Vargas, E.; Latorre, M.; Morales, E.; Vásquez, C.; Arenas, F. Synthesis and antibacterial activity of metal(loid) nanostructures by environmental multi-metal(loid) resistant bacteria and metal(loid)-reducing flavoproteins. *Front.Microbiol*. **2018,** 15 (9), 959.

[30] Huang, W.; Wu, H.; Li, X.; Chen, T. Facile one-pot synthesis of tellurium nanorods as antioxidant and anticancer agents. *Chem. Asian. J.* **2016**, 11(16), 2301-11.

[31] Medina, D.; Tien-Streen, W.; Zhang, B.; Huang, X.; Vernet, A.; Nieto-Argüello, A.; Cholula-Díaz, J.L.; Martínez, L.; Huttel, Y.; Ijué, M.; García-Martín, J.M.; Webster, T.J. Citric juice-mediated synthesis of tellurium nanoparticles with antimicrobial and anticancer properties. *Green Chem.,* **2019**, 21, 1982-1998.

[32] Shakibaie, M.; Adeli-Sardou, M.; Mohammadi-Khorsand, T.; Zeydabadi-Nejad, M.; Amirafzali, E.; Amirpour-Rostami, S.; Ameri, A.; Forootanfar, H. Antimicrobial and antioxidant activity of the biologically synthesized tellurium nanorods; a preliminary In vitro study. *Irani J. Biotech.*, **2017**, 15(4), 268-276.

[33] Gómez-Gómez, B.; Arregui, L.; Serrano, S.; Santos, A.; Pérez-Corona, t.; Madrid, Y. Selenium and tellurium-based nanoparticles as interfering factors on Quorum

sensing-regulated processes: violacein production and bacterial biofilm formation. *Metallomics* **2019**, 11, 1104-1114.

[34] Gómez-Gómez, B.; Sanz-Landaluze, J.; Pérez-Corona, M.T.; Madrid, Y. Fate and effect of in-house synthesized tellurium based nanoparticles on bacterial biofilm biomass and architecture. Challenges for nanoparticles characterization in living systems. *Sci. Total Environ*. **2020**, 719, 137501.

[35] Corte-Rodríguez, M.; Blanco-González, E.; Bettmer, J.; Montes-Bayón, M. Quantitative Analysis of Transferrin Receptor 1 (TfR1) in Individual Breast Cancer Cells by Means of Labeled Antibodies and Elemental (ICP-MS) Detection. *Anal. Chem.* **91**, 15532-15538.

[36] Borguese, B.; Brucale, M.; Fortunato, G.; Lanzi, M.; Mezzi, A.; Valle, F., Cavallini, M.; Zannoni, D. Extracellular production of tellurium nanoparticles by the photosyntetic bacterium Rhodobacter capsulatus. *J. Hazard. Mater.* **2016**, 309, 202-209.

[37] Zare, B.; Faramarzi, M.A.; Sepehrizadeh, Z.; Shakibaie, M.; Rezaie, S.; Shahverdi, A.R. Biosynthesis and recovery of rod-shaped tellurium nanoparticles and their bactericidal activities. *Mater. Res. Bull.* **2012**, 47, 3719-3725.

[38] Shakibaie, M.; Adeli-Sardou, M.; Mohammadi-Khorsand, T.; Zeydabadi-Nejad, M.; Amirafzali, E.; Amirpour-Rostami, S.; Ameri, A.; Forootanfar, H. Antimicrobial and antioxidant activity of the biologically synthesized tellurium nanorods; a preliminary In vitro Study. *Iran. J. Biotechnol.* **2017**, 15, e1580.

[39] Vaigankar, D.C.; Dubey, S.K.; Mujawar, S.Y.; d´Costa, A.; Shyama, S.K. Tellurite biotransformation and detoxification by Shewanella baltica with simultaneous synthesis of tellurium nanorods exhibiting photo-catalytic and anti-biofilm activity. *Ecotox. Environ. Safe.* **2018**, 165, 516-526.

[40] Kim, D.H.; Kanaly, R.A.; Hur, H.G. Biological accumulation of tellurium nanorod structures via reduction of tellurite by Shewanella oneidensis MR-1. *Bioressour. Technol.* **2012**, 125, 127-131.

[41] Doherty, G.J.; McMahon, H.T. Mechanisms of endocytosis. *Ann. Rev. Biochem.* **2009**, 78, 857-902.

[42] Laborda, F.; Bolea, E.; Jiménez-Lamana, J. Single Particle Inductively Coupled Mass Spectrometry: A powerful tool for nanoanalysis. *Anal. Chem.* **2014**, 86, 2270-2278.

[43] Kalomista, I.; Keri, A.; Unqor, D.; Csapó, E.; Dékány, I.; Prohaska, T.; Galbács, G. Dimensional characterization of gold nanorods by combining millisecond and microsecond temporal resolution single particle ICP-MS measurements. *J. Anal. At. Spectrom*. **2017**, 32, 2455-2462.

[44] Abad-Álvaro, I.; Peña-Vázquez, E.; Bolea, E.; Bermejo-Barrera, P.; Castillo, J.R.; Laborda, F. Evaluation of Number concentration quantification by single particle inductively coupled plasma mass spectrometry microsecond vs millisecond dwell times, *Anal. Bioanal. Chem*. **2016**, 408, 5089-5097.

Figure 1.

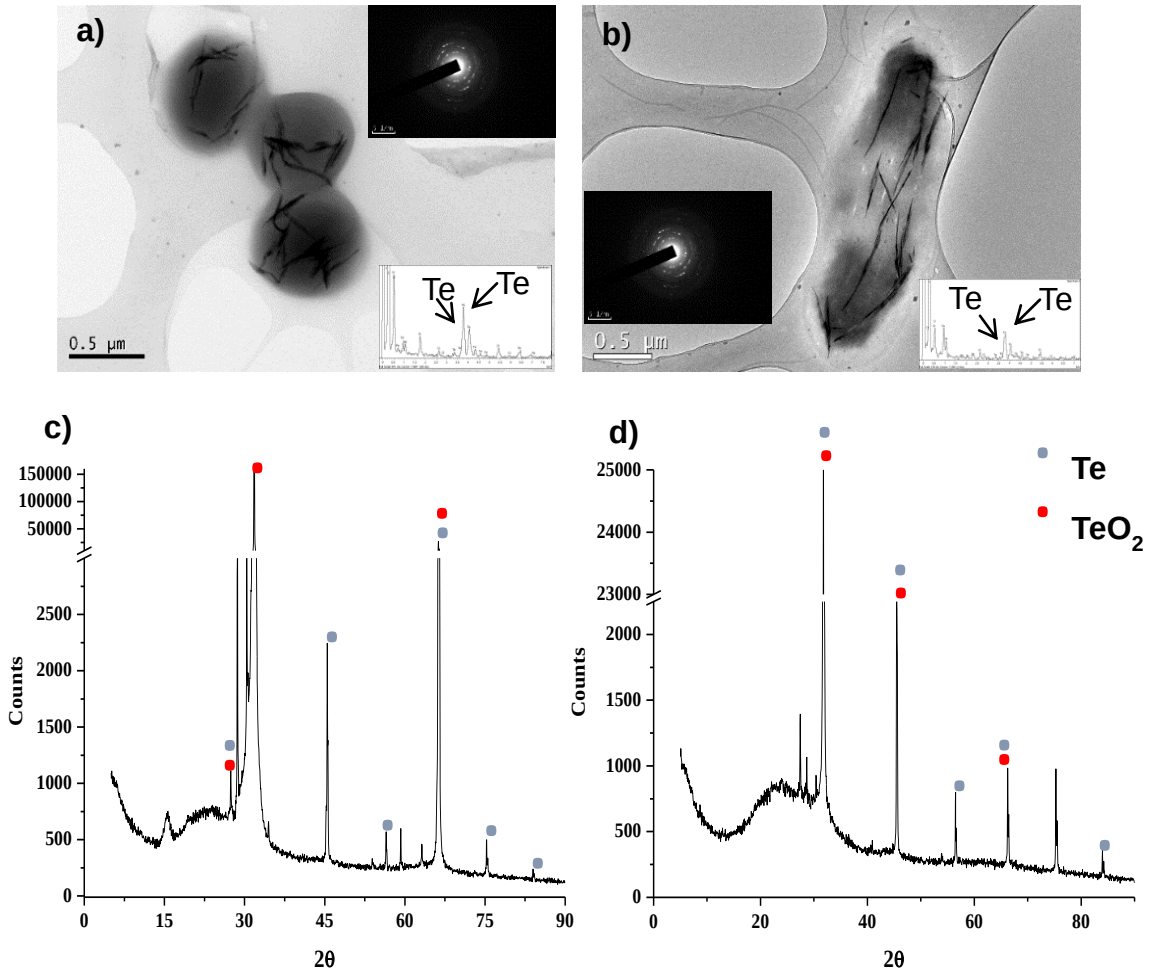

Figure 2.

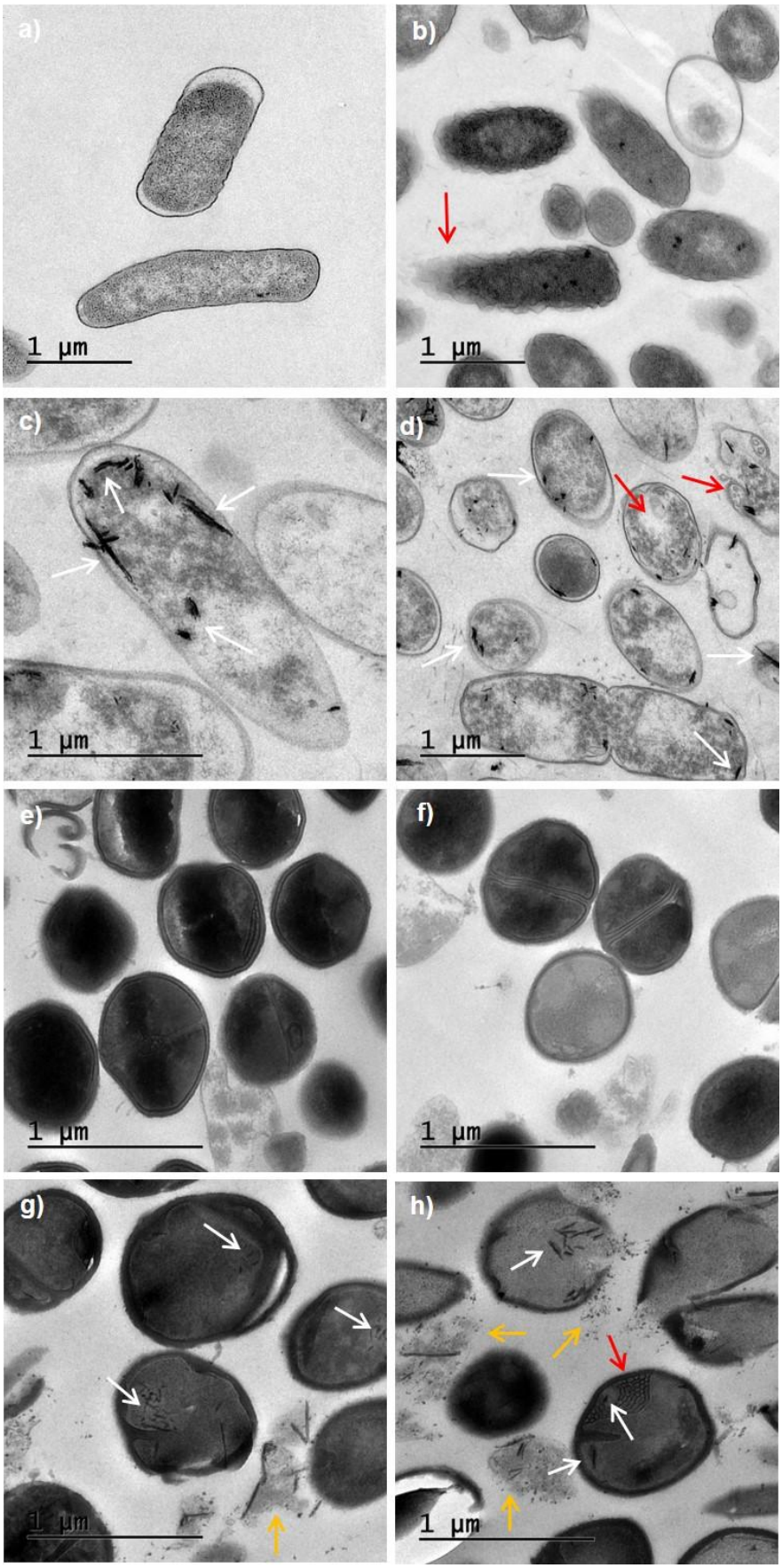

Figure 3.

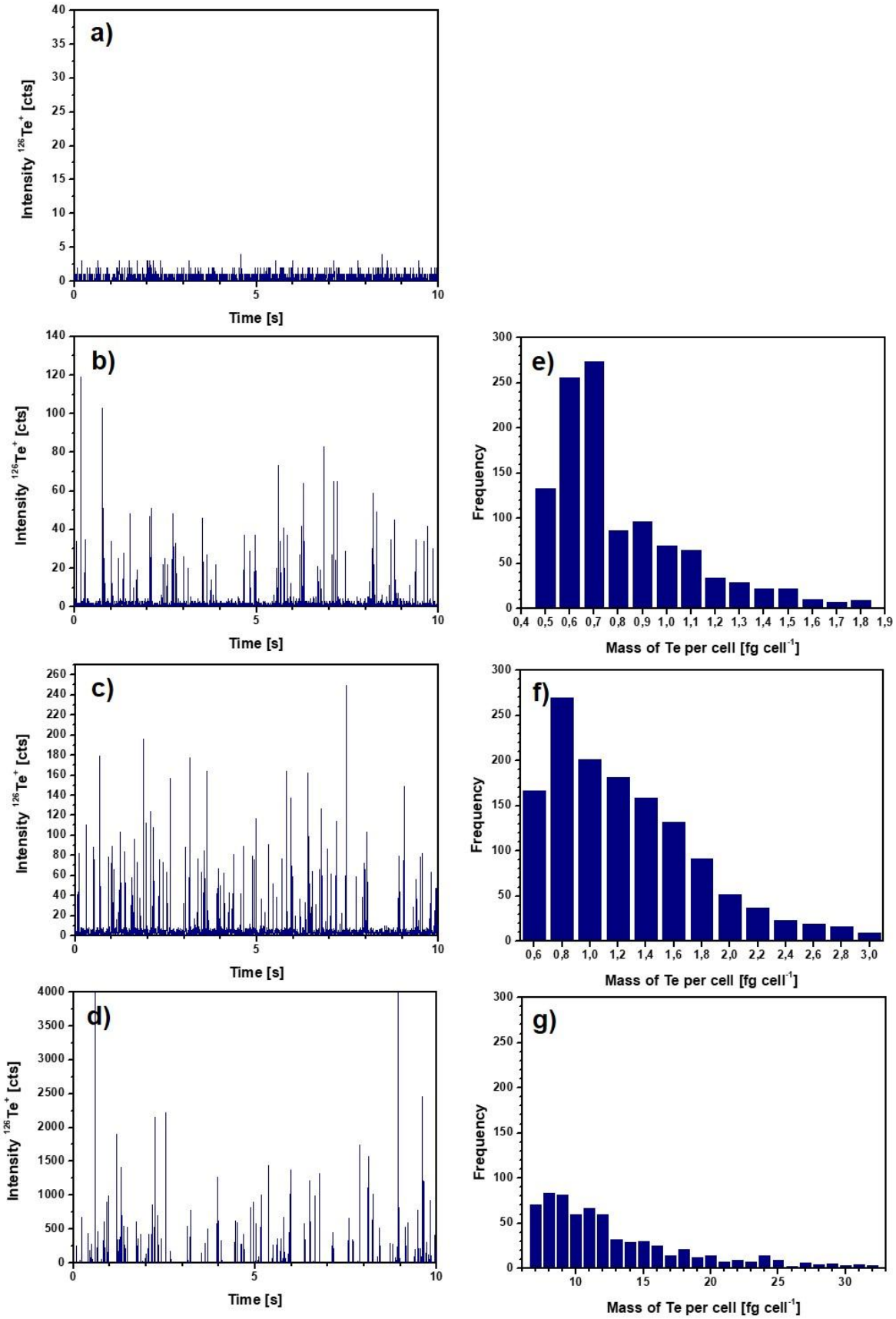
a)
b)
c)
d)
e)
f)
g)
Intensity $^{126}Te^+$ [cts]
Time [s]
Frequency
Mass of Te per cell [fg cell^{-1}]

Figure 4.

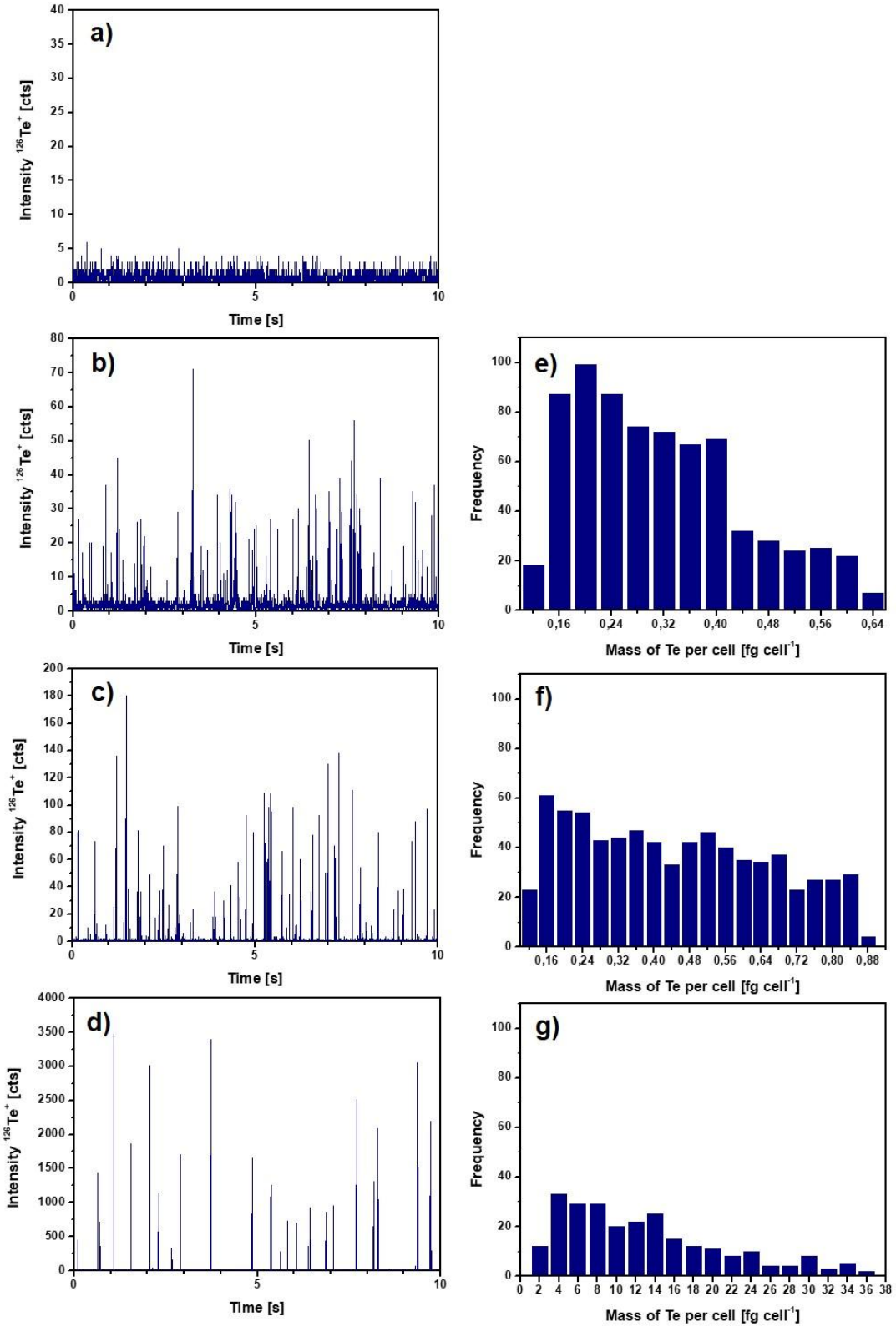
a)
b)
c)
d)
e)
f)
g)
Intensity $^{126}Te^+$ [cts]
Time [s]
Frequency
Mass of Te per cell [fg cell^{-1}]

Figure 5.

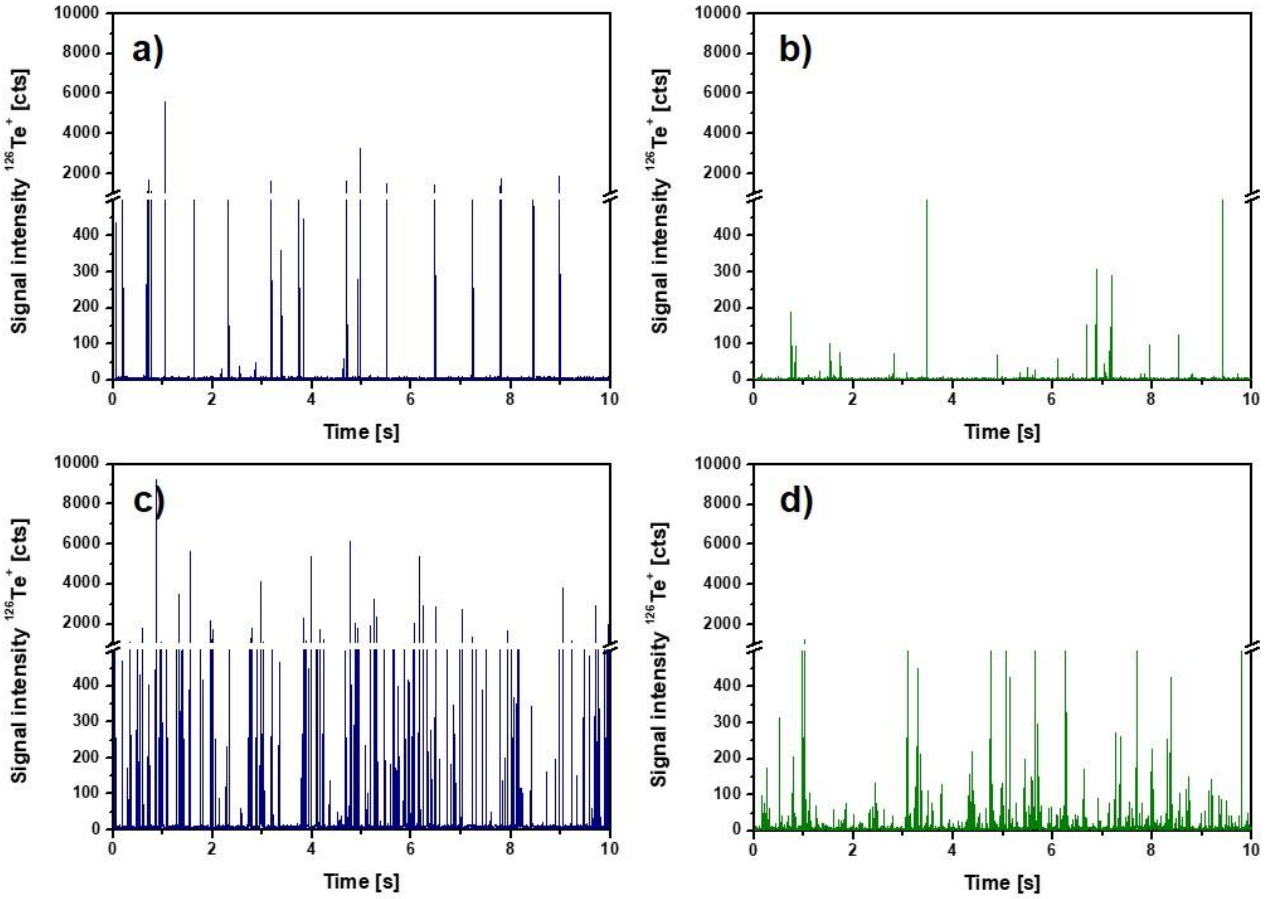
a)
b)
c)
d)
Signal intensity $^{126}Te^{+}$ [cts]
Time [s]
10000
8000
6000
4000
2000
400
300
200
100
0
0
2
4
6
8
10

Figure 6.

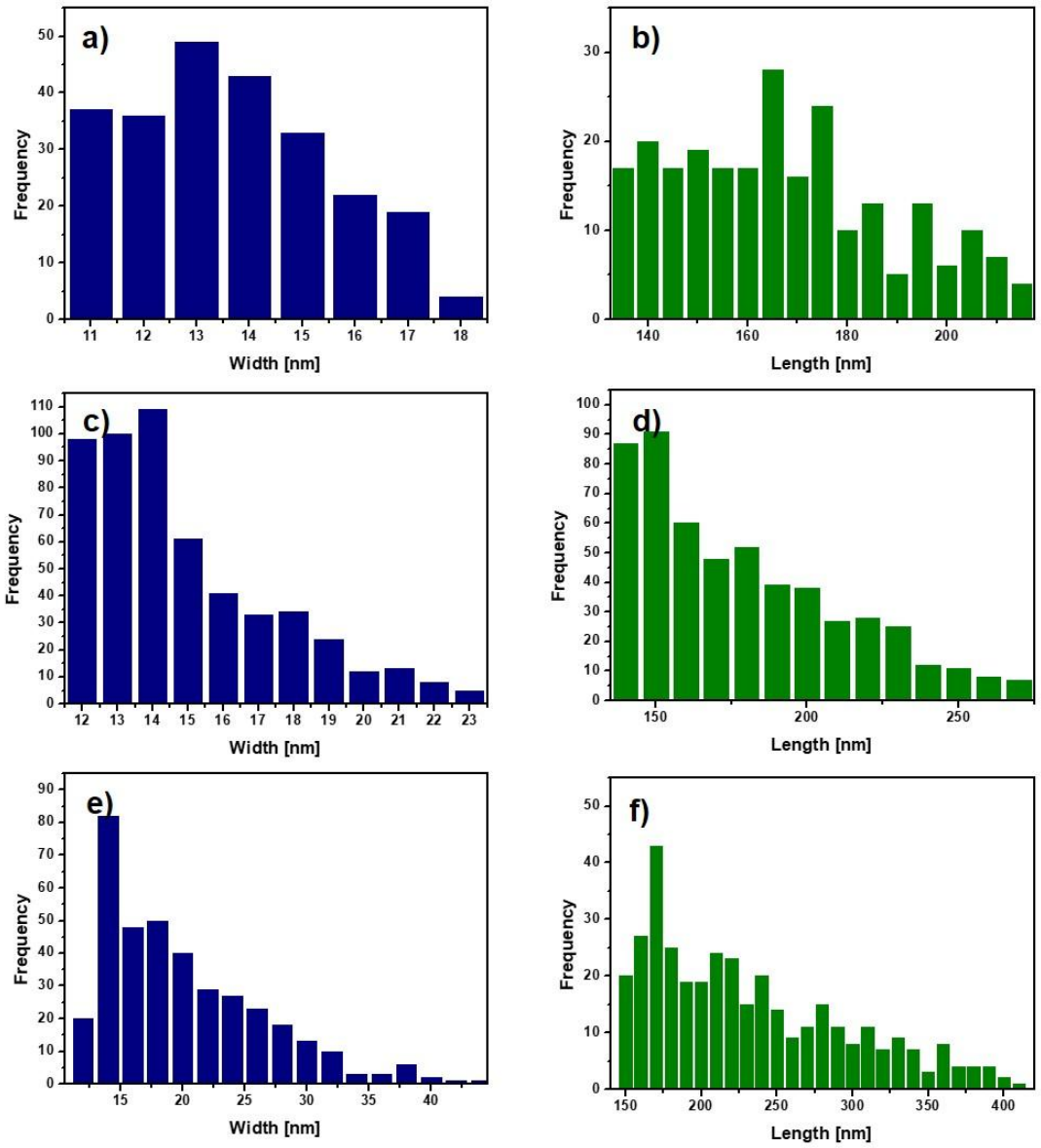
a)
Frequency
Width [nm]
b)
Frequency
Length [nm]
c)
Frequency
Width [nm]
d)
Frequency
Length [nm]
e)
Frequency
Width [nm]
f)
Frequency
Length [nm]

Figure 7.

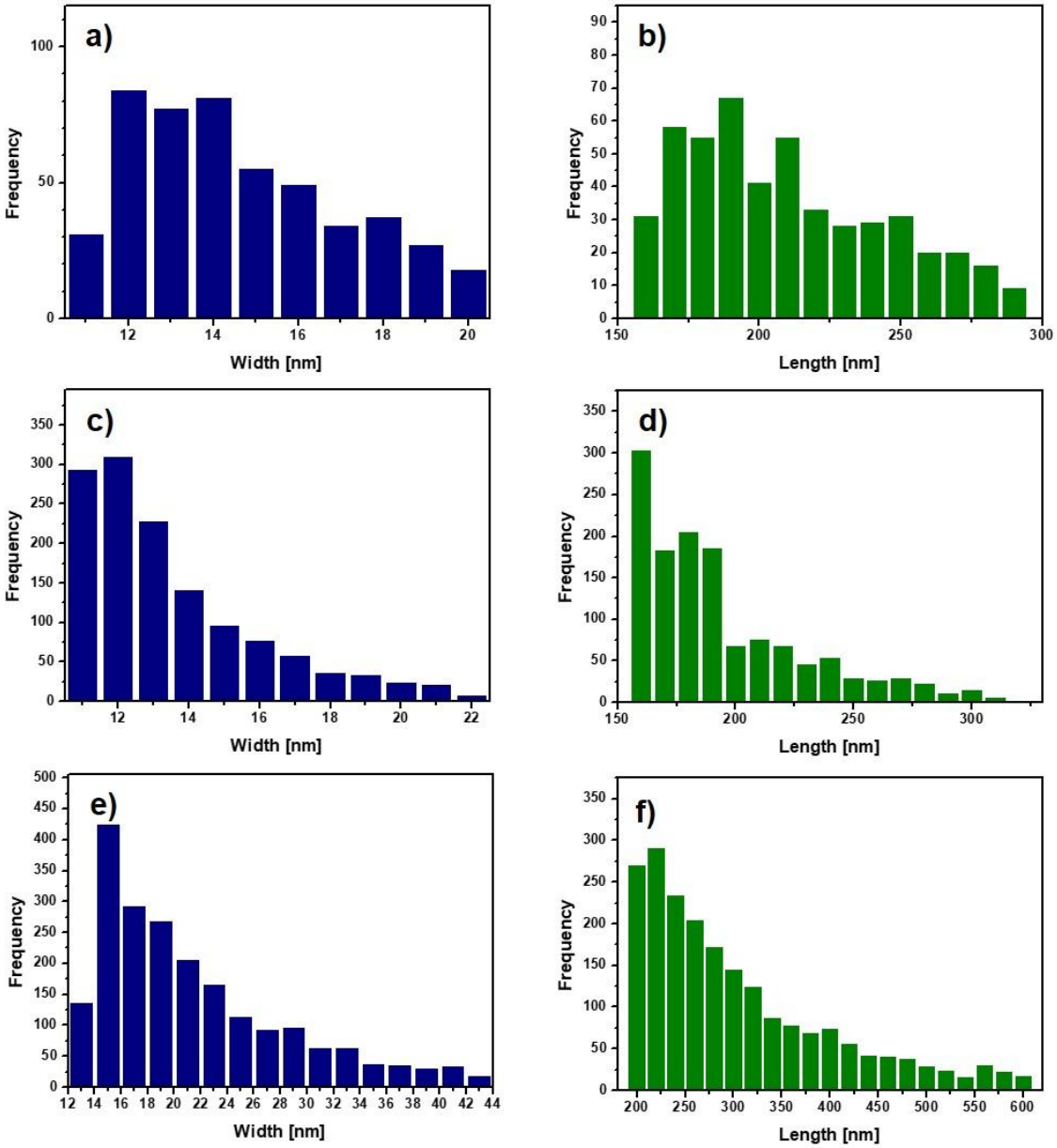
a)
Frequency
Width [nm]
b)
Frequency
Length [nm]
c)
Frequency
Width [nm]
d)
Frequency
Length [nm]
e)
Frequency
Width [nm]
f)
Frequency
Length [nm]

Electronic Supplementary Material (online publication only)

Click here to download Electronic Supplementary Material (online publication only): supporting information revised.docx

Combined single cell and single particle ICP-TQ-MS analysis to quantitatively evaluate the uptake and biotransformation of tellurium nanoparticles in bacteria

Beatriz Gomez-Gomez[1], Mario Corte-Rodríguez[2], Mª Teresa Perez-Corona[1], Jörg Bettmer[2], María Montes-Bayón[2], Yolanda Madrid[1,*]

[1] Complutense University of Madrid, Dept of Analytical Chemistry, Faculty of Chemistry. Avda. Complutense s/n 28040, Madrid. Spain

[2] University of Oviedo, Dept. of Physical and Analytical Chemistry and Instituto de Investigación Sanitaria del Principado de Asturias (ISPA), C/ Julián Clavería 8, E-33006 Oviedo, Spain.

*Corresponding Author:

Prof. Yolanda Madrid Albarran
Dept. of Analytical Chemistry
Faculty of Chemistry
Universidad Complutense de Madrid
E-28040 Madrid, Spain
Phone: +34913945145
Fax: +34913944329
e-mail: ymadrid@quim.ucm.es

Abstract

Assessing the impact of nanoparticles in living systems implies a proper evaluation of their behaviour at single-cell level. Due to the small size of nanoparticles, their accumulation, transformation and location within single cells is challenging. In this work, the combination of single cell/single particle triple quadrupole inductively coupled plasma mass spectrometry (SC/SP-ICP-TQ-MS) analysis along with X-ray diffraction (XRD) and transmission electron microscopy (TEM) measurements has been applied to go deeper into the uptake and biotransformation of tellurium nanoparticles (TeNPs) in two bacterial model organisms, *S. aureus* and *E. coli*. The use of SC-ICP-TQ-MS enabled the individual introduction of bacterial cells where tellurium and phosphorous (as constitutive element) were monitored and detected at concentration levels down to femtogram (fg) per cell. *S.aureus* uptake of TeNPs was 0.5-1.9 fg Te $cell^{-1}$ and 7-30 fg Te $cell^{-1}$ in presence of 0.5 and 15 mg Te L^{-1} of TeNPs, respectively, whereas for *E. coli*, the amount of Te ranged from 0.08 to 0.88 fg Te $cell^{-1}$ and from 2 to 36 fg Te $cell^{-1}$ in presence of 0.5 and 15 mg Te L^{-1} of TeNPs, respectively. TEM and XRD analysis confirmed the occurrence of TeNPs biotransformation (from nanospheres to nanorods) as the nanoparticles were incorporated into both bacterial strains. Finally, SP-ICP-MS analysis after cell lysis was applied to determine the number of particles/rods per bacteria cell and to perform the dimensional characterization of the rod-shaped TeNPs. The results obtained clearly confirmed high cell-to-cell variability in terms of Te nanorods dimensions and TeNPs uptake. To the best of our knowledge, this is the first time that SC/SP-ICP-TQ-MS along with TEM and XRD analysis have been applied to investigate, quantitatively, nanoparticle uptake in bacterial cells and to estimate the dimensions of biogenic Te nanorods.

Keywords: single cell ICP-MS; single particle ICP-MS; Tellurium nanoparticles; nanorods; *S. aureus*; *E. coli.*

1. Introduction

Application of metal/metalloid-based nanoparticles is increasing in areas directly related to our daily life. For example, nanoparticles are in the formulation of personal care and food products or textiles. Moreover, nanoparticles have attracted a great interest in medicine due to their potential as antimicrobial and drug delivery agents [1-5]. Unfortunately, the release of these nanomaterials into the environment is nowadays a matter of concern. Therefore, there is a need to elucidate the real impact of nanoparticles on ecosystems and human health, including a proper evaluation about their behaviour at single-cell level [6]. For this aim, there is also a limitation in the existing analytical tools. In fact, most of the reported studies on this topic estimate average contents of nanoparticle uptake in the entire cell population by performing classical bulk analysis of a large amount of cells after dissolution [7,8]. As a matter of fact, this approach does not provide information on cell to cell variability. Quantifying metal/metalloid based nanoparticles accumulation at single cell level is not an easy task due to both, the lack of appropriate methodologies and the difficulties found when performing cell lysis [9]. Moreover, this kind of studies becomes even more complicated when nanoparticles transformations in biological media take place [10].

Lately, ICP-MS-based analytical techniques for nanoparticles and cells determination such as single-particle ICP-MS (SP-ICP-MS) and single-cell ICP-MS (SC-ICP-MS), respectively, have emerged as powerful techniques for quantitatively assessing the impact of nanoparticles in living systems. SP-ICP-MS has been widely employed for sizing and quantifying nanoparticles in terms of number of nanoparticles in a wide range of matrices including consumer products, medical devices, biological tissues and environmental samples [11-15]. SC-ICP-MS follows a similar principle than SP-ICP-MS and is used to detect and quantify the metal content within individual cells [16]. In this approach, cells are directly nebulized (nowadays often using micro-flow nebulizers [17]) or micro-droplets dispensed into the plasma [18]. Then, the ions generated from

single cells are individually detected by applying high time resolution. In order to be successful in this type of analysis, it is crucial to obtain diluted cell suspensions and to introduce them into the plasma in the most efficient manner. For the latter purpose, special sample introduction systems are continuously being developed and improved by combining different micro-flow nebulizers with total consumption spray chambers [17,19, 20].

SC-ICP-MS has been successfully applied to evaluate the uptake of trace elements and metal-based nanoparticles by single human, algae or yeast cells [21-24]. However, its application to bacteria has been scarce, in spite of the fact that bacteria are crucial model organisms for assessing the impact of nanomaterials in the environment [25]. The main difference when performing analysis of human, algae, yeast or bacterial cells by SC-ICP-MS is the size of the different type of cells. Bacterial cells have a size smaller than algae, yeast or human cells. However, this aspect is not a problem; it could be actually an advantage. On the other hand, it is known that yeast cells are more resistant to mechanical disruption than bacterial cells. So, the main challenge found when analysing bacterial cells by SC-ICP-MS is to keep their physical integrity during their pass through the ICPMS system, from sample introduction system to the plasma. Although, this problem is inherent when analysing any type of cells by SC-ICP-MS it is even more accused when working with bacterial cells. The limited used of SC-ICP-MS for bacteria cells analysis could be also attributed to the novelty of the technique and consequently many of its applications are still under development.

In addition, most of the studies related to the quantification of nanoparticle uptake and distribution at single cell level have focused on well-known commercial nanoparticles such as silver or gold. Recently, tellurium-based nanoparticles (TeNPs) are being applied in various industrial fields such as the production of solar panels, glasses, new-generation rechargeable batteries and electronic devices as well as for environmental

remediation and biomedical applications [26-32]. However the knowledge about their impact on environment and living systems is quite limited

Although, the accuracy, precision and robustness of SP-ICP-MS have been clearly demonstrated, limitations arise when nanoparticles are far from having a spherical morphology, as calculations on their size distribution and concentration are based on the assumption that nanoparticles are spherical in shape. This limitation implies a serious problem when evaluating the behaviour of nanoparticles in living systems, as nanoparticles may undergo morphological changes when they are in contact with complex systems [33, 34].

Therefore, in this work we aim to study the fate and uptake of tellurium based nanoparticles (TeNPs) in two widely employed bacterial model organisms, *Staphylococcus aureus* and *Escherichia coli*, by combined single cell and single particle ICP-TQ-MS along with electron microscopy (TEM) and X-ray diffraction (XRD). The work has been divided into three parts: 1) nanoparticle characterization before and after being added to bacterial culture by TEM and XRD measurements in order to investigate morphological and compositional changes that nanoparticles may suffer as consequence of their interaction with bacteria, 2) quantification of accumulated TeNPs in individual bacterial cells at different exposure levels by performing SC-ICP-MS analysis, and 3) dimensional characterization of tellurium nanorods formed thorough the interaction of bacteria with the originally spherical TeNPs by employing TEM and SP-ICP-MS measurements. To the best of our knowledge, this is the first time that SC-ICP-MS and SP-ICP-MS along with TEM and XRD analysis have been applied to investigate nanoparticle uptake in bacterial cells and to estimate the dimensions of Tellurium nanorods.

2. Materials and Methods

2.1 Synthesis and characterization of tellurium nanoparticles (TeNPs)

Tellurium nanoparticles (TeNPs) were synthesized following the procedure previously reported by Gómez-Gómez et al. Briefly, the chemical reduction of potassium tellurite (K_2TeO_3, Sigma Aldrich) was carried out with gallic acid (Sigma Aldrich) in presence of hydroxyethyl cellulose (HEC, Sigma Aldrich) as coating agent [33,34]. After that, TeNPs were purified through a dialysis process. The characterization of these nanoparticles in terms of size, size distribution, morphology or composition, as well as their properties in solution (hydrodynamic diameter, the zeta potential and number particle concentration) has been already described in a previously published work [34]. Therefore, for this study, the nanoparticles synthesized were only submitted to a routine characterization before each experiment employing TEM (JEOL JEM 2100, Peabody, MA, USA) equipped with energy-dispersive X-ray spectroscopy (EDXS) microanalysis composition system (Oxford Instruments, High Wycombe, UK). Moreover, TeNPs were also characterized in the bacterial culture medium, Luria Bertani broth (LB), with the aim of assessing their stability under the same conditions as the subsequent studies.

On the other hand, Te nanorods found in bacterial cultures were also characterised by TEM. Image J software was used to obtain the values of width and length of the rod-shaped TeNPs from a representative amount of TEM images. In addition, X-ray diffraction pattern for rod-shaped TeNPs was obtained using a Panalytical X´PERT-MPD X-ray diffractometer (Malvern Panalytical, Ma, USA) operated at a voltage of 40 keV, 20 mA of current and 1.541 A of Cu Kα radiation.

2.2 Bacteria culture conditions and exposure to TeNPs

S. aureus (ATCC 29213) and *E. coli* (ATCC 25922) were cultured in Luria-Bertani (LB) medium and grown overnight at 37ºC under stirring (120 rpm). The obtained bacterial suspensions were diluted with LB solution until reaching an optical density (OD) of 0.1 at 620 nm. Then, bacterial cells were exposed to 0.5, 1 and 15 mg Te L^{-1} as TeNPs during 18h at 37ºC and 120 rpm. Non-incubated bacterial cells (control) were also treated in the same way. Three biological replicates were carried out for each experiment. Afterwards, bacterial cultures were centrifuged at 7000 rpm during 3 min. The supernatants were removed and the bacterial cell pellets were washed twice with Milli-Q water. Aliquots of 100 mg of bacterial pellet underwent an acid digestion with HNO_3/H_2O_2 (3:1). Finally, tellurium concentration in the digested pellet was measured by the triple quadrupole based Thermo iCAP TQ ICP-MS (Thermo Fisher Scientific, Bremen, Germany) using the single quadrupole mode. The ICP-MS was equipped with a Micro Mist nebulizer, a cyclonic spray chamber (both from Thermo Fisher Scientific) and an auto-sampler ASX-560 (Teledyne CETAC Technologies, Omaha, NE, USA). Furthermore, another aliquot from each bacterial culture was selected and monitored by TEM as described in the following section.

2.3 TeNPs internalization in bacteria by transmission electron microscopy (TEM)

Bacterial cells were exposed to different concentrations of TeNPs (as indicated above), then harvested by centrifugation at 7000 rpm during 3 min and finally washed with phosphate-buffered saline (PBS) (Sigma-Aldrich, St. Louis, MO, USA). Samples were then prepared for TEM observations through a process including fixation, dehydration, and embedding in a resin matrix. Briefly, bacterial cell pellets were fixed *in situ* with glutaraldehyde (2.5% v/v) (Sigma-Aldrich, St. Louis, MO, USA) and p-formaldehyde (4% v/v) (Sigma-Aldrich, St. Louis, MO, USA) in PBS at 4ºC for 4h. The resulting

mixture was subsequently treated with osmium tetraoxide (1% v/v) during 1h at room temperature under darkness and then dehydrated in graded acetone series (from 30% to 100 %). Afterwards, pellets were treated first with a mixture of resin:acetone, and finally, with 100% resin. The resulting blocks were incubated at 65ºC for 48h. Finally, ultrathin sections of samples were cut and examined by TEM.

2.4 Flow cytometry analysis

Flow cytometry measurements were performed in bacteria cell suspensions, in presence and absence of nanoparticles , to determine the percentage of viable and non-viable cells and to establish the number of bacterial cells with the aim of calculating the transport efficiency of the sample introduction system. For cytometry analysis, bacterial cultures exposed to TeNPs were washed three times with Tris-buffered saline (TBS, Sigma-Aldrich, St. Louis, MO, USA) solution and diluted with Milli-Q water until a bacterial cell concentration close to 10^5 cells mL^{-1} was achieved. After that, diluted bacterial cell suspensions were incubated with SYTO 9 and propidium iodide (PI) fluorescent dyes (Thermo Fisher Scientific, MA, USA) during 15 min. Finally, analyses were performed with a Flow Cytoflex S from Beckman Coulter (Brea, CA, USA).

2.5 Single cell analysis by ICP-TQ-MS

Bacterial cell suspensions obtained from the exposure experiments were washed three times with TBS and diluted with Milli-Q water to get a concentration in number of cells of approximately 10^5 cells mL^{-1}. Single-cell analysis was performed by using the iCAP TQ ICP-MS equipped with a high performance concentric nebulizer (HPCN) combined with the total consumption spray chamber (High Sensitivity Single-Cell Sample Introduction System for ICP-MS, Glass Expansion, Port Melbourne, Australia). Samples and rinsing solutions were introduced into the plasma at a flow rate of 10 µL min^{-1} using the MVX-7100 µL Workstation (Teledyne CETAC Technologies, Omaha,

NE, USA). Instrumental and data acquisition parameters are listed in Table S1. Measurements were carried out under time resolved analysis mode during 2 min per analysis with a dwell time of 5 ms and by selecting ^{126}Te as monitoring isotope. Furthermore, constitutive phosphorous chosen as constitutive cell element was measured as oxide ($^{31}P^{16}O^{+}$) in the triple quadrupole mode by using oxygen as reaction gas in a separate run. Transport efficiency of calibration standards was calculated by analysing citrate stabilized gold nanoparticle (AuNPs, nominal diameter 30 nm) standard (RM 8012) obtained from the NIST (Gaithersburg, MD, USA). Moreover, CyTOF Calibration Beads (Fluidigm Corporation, San Francisco, CA, USA) containing europium, at a particle number concentration of 33000 mL^{-1} (Fluidigm Corporation, San Francisco, CA, USA) were also employed to determine cell transport efficiency daily [35]. In order to performTe mass quantification by SP-ICP-MS analysis, a calibration curve of ionic tellurium was prepared daily within a concentration range from 0 to 50 µg L^{-1} with a tellurium standard for ICP obtained from Sigma Aldrich (St. Louis, MO, USA).

Data treatment of SC-ICP-MS analysis was carried out by applying an iterative procedure previously reported [19]. Briefly, the procedure consisted of selecting all data points that were three times the standard deviation (3σ) above the mean. The mean value was previously calculated by considering all the entire data set. The remaining data set was subjected again to the same procedure. The iterative procedure is repeated until there were no data points higher than the value of mean plus 3σ, and that value was used as threshold for cell events. Te amount in *S. aureus* and *E. coli* cells at a single-cell level was determined by applying Equation 1 [26]:

$$m_c = \frac{\eta \cdot F \cdot t \cdot I}{b} \qquad \text{(Equation 1)}$$

where m_c is the mass of the element in the cell, η is the transport efficiency for the liquid standards calculated using RM 8012 in the single particle mode, F is the sample

flow rate, t is the integration time, I is the count rate of Te, and b is the slope of the Te calibration curve previously measured.

Finally, to validate the data obtained from SC-ICP-TQ-MS analysis, the uptake of TeNPs by *S. aureus* and *E. coli* was assessed by means of ICP-TQ-MS (in single quad mode) after cell lysis, and referred to the number of bacteria present in the sample and counted by flow cytometry.

2.6 Bacteria cell disruption and single-particle ICP-MS (SP-ICP-MS) analysis of cell lysates

Bacterial cells were disrupted mechanically by using 0.5 mm glass beads (Merck Millipore, Darmstadt, Germany) and by adapting the procedure described by Álvarez-Fernández et al [23] . In this sense, 1 mL of bacterial cell suspensions was mixed with 734 mg of glass beads (500 µm of diameter) in an Eppendorf tube. Afterwards, the mixture was submitted to 5 min Vortex agitation followed by 10 min of sonication by means of an ultrasonic bath. The procedure was repeated twice for *E. coli*, but up to six cycles were needed to disrupt the *S. aureus* cells. Subsequently, cell debris and unbroken bacteria cells were removed appropriately by applying a centrifugation step at 2,000 g for 2 min. Particle mass quantification of TeNPs inside bacteria cells or adhered to bacterial membrane after bacterial cell disruption was performed by SP-ICP-MS and by applying the same procedure as for SC-ICP-TQ-MS analysis (described in section 2.5).

3. Results and Discussion

3.1 Accumulation and morphological transformation of TeNPs by *Staphylococcus aureus* and *Escherichia coli*.

The synthesis of the TeNPs resulted in the formation of spherical particles with a diameter of (125 ± 40) nm and with a composition of 80 % TeO_2 and 20 % Te. A

detailed characterization of the synthesized TeNPs is summarized in the Supporting Information (Figure S1).

The uptake of TeNPs by *S. aureus* and E. coli was assessed after their exposure to 0.5, 1 and 15 mg Te L-1 as TeNPs during 18h at 37ºC following the conditions described previously. Exposure levels were chosen based on previous studies published in the literature by the authors [33,34] who investigated the behaviour of TeNPs on bacterial biofilms developed by *S.aureus* and *E. coli*. In the current study the effect of TeNPs on *S. aureus* and *E. coli* was evaluated by selecting the same levels of TeNPs exposure as in previous studies but with the difference that bacterial cells were growth in planktonic mode.

The amount of Te accumulated was calculated by acid digestion of the bacterial pellet followed by ICP-TQ-MS analysis in single quad mode. The highest accumulation percentages were found for *S. aureus* reaching nearly 100 % for all levels of TeNPs administered, whereas the accumulation percentages in *E. coli* varied between 28% and 48% depending on the TeNPs concentration supplemented to the bacterial culture (Table 1).

Flow cytometry analyses were also performed in order to study the effect of TeNPs on *E. coli* and *S. aureus* viability. As shown in Table S2, around 80%-90% of bacterial cells were viable in case of *S. aureus* and *E. coli* regardless the amount of TeNPs supplemented.

It is important to notice that a change in the colour of the culture medium - from almost colourless to deep black - was observed when the highest concentration of TeNPs was supplemented to both bacterial strains. In contrast, no variation in the culture medium colour was observed when TeNPs were dispersed in LB medium in absence of bacteria. The observed colour changes were associated with the appearance of tellurium nanorods as shown in Figures 1a and b. The presence of tellurium nanorods

was only detected in presence of high particle concentration of 15 mg L^{-1}, but not at 0.5 and 1 mg Te L^{-1} levels. This fact can be explained as 0.5 and 1 mg Te L^{-1} were very low Te levels to be observed by TEM. The electron diffraction pattern composed by concentric rings presented in TEM images (Figures 1a and b) confirmed the crystalline structure of the rod-shape tellurium nanoparticles. The morphological change observed (from spherical to nanorod shape) can be linked to a detoxification mechanism as it has been also reported for SeNPs and TeNPs in different bacteria strains, suggesting a low toxicity against bacteria of rod-shape nanoparticles compared to spherical ones [36-40]. To the best of our knowledge, the morphological transformation of TeNPs from spheres to nanorods after being exposed to *S. aureus* and *E. coli* planktonic cells has not been reported to date.

Size of tellurium nanorods was determined by counting more than 200 individual particles from different TEM images and by employing the Image J software. It was found that the length and width of Te nanorods in *E. coli* experiments were (303 ± 23) nm and (26 ± 10) nm, respectively, with an aspect ratio of around 12. The respective data for *S. aureus* were (267 ± 129) nm and (21 ± 8) nm with an aspect ratio of around 14. Additionally, the phase and composition of tellurium nanorods were also determined by X-ray diffraction. Figures 1c and 1d display XRD spectra obtained from *S. aureus* and *E. coli* treated with TeNPs. In the case of *S. aureus*, peaks of tellurium nanorods were indexed as cubic phase (Fd-3m space group: 227) and rhombohedral phase (R-3m space group: 166) of Te crystal and as orthorombic phase of crystalline TeO_2 (Pnma space group: 62). These values agreed well with the standard literature data (card number 04-002-3701, 04-015-6838 and 04-022-7519 respectively). Moreover, XRD analysis indicated that tellurium nanorods were composed of 99% $Te0_2$ and 1% Te. With respect to *E.coli,* peaks of tellurium nanorods were assigned to cubic phase (Fd-3m space group: 227) and monoclinic phase (P21 space group: 4) of Te crystal and orthorombic phase of TeO_2 (Pnma space group: 62) which is in good

agreement with the standard literature data (card number 04-002-3701, 04-007-2056 and 04-022-7519 respectively). XRD measurements indicated that tellurium nanorods were also composed of 99% TeO_2 and 1% Te.

The results obtained clearly demonstrate important morphological and compositional changes in nanoparticles as they interact with bacterial cells. Nanoparticle adhesion to bacteria cell surface or internalization into bacteria cells are two of the most plausible mechanisms that may happen as consequence of the bacterial exposure to nanoparticles interaction. TEM images from Figures 1a and b have evidenced that TeNPs interact with bacteria surface. Unfortunately, TEM images were not clear enough to ensure whether nanoparticles were inside of bacteria cell or just attached to bacterial membranes. To correctly locate nanoparticles in relation to bacterial cells, TEM images of chemically fixed bacteria cells (by applying the procedure described previously) were acquired to corroborate the information gathered from TEM images previously described (Figure 1a and b). Figure 2 shows sectioned TEM images of *E. coli* and *S. aureus* in presence of 0, 1 and 15 mg Te L^{-1} as TeNPs. In *E. coli* experiments, it is difficult to ensure the presence of nanoparticles inside the bacteria at 1 mg Te L^{-1} as TeNPs, due to the fact that the concentration of tellurium was too low to be detected by TEM microscopy (Figure 2b). However, bacterial cell surface damage can be clearly detected (Figure 2b) in comparison to the control cells (Figure 2a). Concerning to *E. coli* treated with 15 mg Te L^{-1}, tellurium nanorods can be found (highlighted with white arrows) either on the surface of the bacterial cell wall or inside the bacterial cell, probably in the cytoplasm (Figures 2c and d). Morphological changes in bacteria cell surface along with vesicles and ruffled extensions of the bacterial plasma membrane (red arrows) are detected. Endocytosis has been described as one of the most likely mechanism of nanoparticles internalization into cells [41]. Sectioned TEM images of *E. coli and S. aureus* treated with the lowest level of TeNPs (0.5 mg Te L^{-1} as TeNPs) are depicted in Figure S2 of the Supporting Information.

Similarly, in the case of *S. aureus*, no particles attached to the bacteria membrane or inside the bacteria were observed at 1 mg Te L^{-1} as TeNPs (Figure 2f). After incubation with 15 mg Te L^{-1} as TeNPs (Figure 2g) rod-shaped tellurium nanoparticles (white arrows) were present either associated to bacteria membrane or inside bacterial cells. Once again, vesicles as consequence of an endocytosis process were perceived (red arrows, Figure 2h). In addition, nanoparticles might induce other membrane deformation and lysis as well as a release of cytoplasmic contents (yellow arrows, Figures 2g and h).

3.2 Quantitative analysis of TeNPs uptake at single cell level.

Up to this point, the uptake and accumulation of TeNPs in *S. aureus* and *E. coli* was measured and averaged within the entire cell population and assuming that all bacterial cells incorporate the same number of nanoparticles. However, it is well known that metals and nanoparticles are heterogeneously distributed in cells. Single-cell ICP-MS has been employed in this work to perform TeNPs uptake profiling at single bacterial cell level. The analytical determination of TeNPs by SC-ICP-MS is challenging since the information about these nanoparticles (physicochemical properties, behaviour in living systems such as cell and bacteria) is really scarce compared to other better characterized as AuNPs and AgNPs [21,24].

For performing SC-ICP-MS analysis, a high performance concentric nebulizer with a total consumption spray chamber was employed. This combination enabled the introduction of intact bacteria into the plasma with a transport efficiency as high as 60 %. No statistically significant differences of transport efficiencies were found either for AuNPs (NIST 8012) or for 2.5 µm polystyrene CyTOF calibration beads loaded with europium as standard suspensions. To ensure that each individual ICP-MS signal corresponds to a single cell, the cell density was adjusted to approximately around 10^5 cells per mL.

Moreover, the efficiency of the cell introduction system was calculated by comparing data from the bacterial cell population, counted by flow cytometry, and the number of cell signals obtained for the constitutive element phosphorus (monitored as $^{31}P^{16}O^{+}$) in the single cell ICP-MS experiments [23]. Under optimal experimental conditions, the cell introduction efficiency was (74 ± 6) % and (85 ± 7) % for *E. coli* and *S. aureus*, respectively. Differences in the percentages of the introduction efficiency might be attributed to differences in bacterial cell size, 2.14±0.52 µm for *E.coli* and 0.74±0.12 µm for *S.aureus* (according to data from TEM micrographs).

The amount of TeNPs (expressed as Te) at single-cell level was calculated by using an external calibration curve obtained with a tellurium standard solution followed by data processing as described in the experimental section. The limit of detection (LOD) was found to be (0.068 ± 0.008) fg Te per cell. Figures 3a-d and 4a-d show time-resolved analyses of $^{126}Te^{+}$ obtained from *S. aureus* and *E. coli* cultures, respectively, after being exposed to TeNPs.

As shown in Figures S3 and S4, the number of phosphorus events decreased with increasing TeNPs concentrations from 2031 to 1503 for *S. aureus* and from 3643 to 427 for *E. coli*. The results show the influence of TeNPs on cell population density being more pronounced in the case of E. coli. On the contrary, a significant number of events, with increasing intensities of $^{126}Te^{+}$ as TeNPs concentration raised, could be observed in Figures 3b-d and 4b-d, whereas no spike signals were detected in the control samples (Figures 3a and 4a). Therefore, those spike signals that fulfil the criterion of being three times higher than the mean value of the background baseline were gathered and transformed into Te mass (fg) per single cell. Mass distribution histograms showing Te mass per individual cell (fg Te per cell) at each supplemented TeNPs concentration are displayed in Figures 3e-g and 4e-g for the two bacterial strains. As it was previously indicated, a LOD value of 0.068 fg Te per cell was obtained in this study which means that we were able to detect levels of Te

accumulated higher than the LOD, such as 0.5, 0.6 or 7 fg Te per cell as shown in in Figures 3g, e and f. We did not detect any concentration below 0,5 fg per cell as the bacterial cells accumulated greater amount of Te than 0.5fg/cell. Similarly, accumulation values much higher than LOD were determined for *E coli* and ranged from 0.8 to 2 fg Te per cell as shown in the frequency histograms depicted in figure 4g, e and f.

As it was expected, the mass of TeNPs accumulated in individual bacteria is heterogeneously distributed for each experimental condition tested. Moreover, results from SC-ICP-TQ-MS analysis in single quad mode confirmed that TeNPs were either internalized or adsorbed onto the bacterial cell wall even at low levels of exposure such as 0.5 and 1 mg Te L-1 as TeNPs. As it was previously mentioned, TEM was not able to visualize the accumulation of TeNPs in bacteria population at these low TeNPs levels of exposure. The average amount of Te per cell varied from (0.77 ± 0.22) fg per cell to (12.80 ± 5.58) fg cell for *S. aureus* and (0.30 ± 0.13) fg per cell to (12.43 ± 4.36) fg per cell for *E. coli* (Table 2).

The percentage of *E. coli* cells containing Te increased from 35% to 59% for bacterial cells exposed to 0.5 and 1 mg Te L^{-1} up to 94% at the highest level of exposure. In the case of *S. aureus*, the percentages increased from 57% to 76% for cells exposed to the lower concentrations up to 100 % at 15 mg Te L^{-1}. ANOVA analysis evidenced statistically significant differences ($P<0.05$) among values for Te amount per cell for those bacteria treated with 0.5 and 1 mg Te L^{-1} compared to 15 mg Te L^{-1} as well as statistically significant differences between the Te amount found in both strains and in the presence of 0.5 and 0.1 mg Te L^{-1} as TeNPs (Table 2). It is important to notice that data in Table 2 is referred only to bacterial cells that accumulate TeNPs. Bacteria cells that did not accumulate TeNPs were not detected by SC-ICP-MS since Te signal was monitored. The total bacterial cell population was estimated by monitoring the phosphorus signal in SC-ICP-MS measurements.

The accuracy of the data provided by SC-ICP-TQ-MS for quantifying Te at individual bacterial cell level was thereafter assessed by combining ICP-TQ-MS in single quad mode after acid digestion (total Te concentration per bacterial cell) and flow cytometry (total bacterial cell population) measurements. As shown in Table 2, there is a good agreement between results obtained by both methods. Consequently, SC-ICP-TQ-MS seems to provide accurate data about the mass of TeNPs uptaken by individual bacterial cells with the advantage of delivering information on the variability from cell to cell

3.3 Determination of the number of TeNPs per individual bacterial cells.

The number of individual particles either internalized or adhered to bacteria wall was determined after the mechanical bacterial cell lysis with glass beads. The performance of the method applied for bacterial cell disruption was assessed by monitoring the signals of phosphorous before and after applying the lysis procedure. Around a (90 ± 4) % and (92 ± 2) % of the cells were disrupted in S. aureus and E. coli experiments, respectively. Furthermore, tellurium was also monitored in a second run. The time resolved analyses for Te in Figure 5 demonstrates that the intensity of the events decreased after applying cell disruption at 15 mg Te L.1. Although this effect was detected for all levels of exposure, it was more pronounced at 15 mg Te L-1 as TeNPs. The results obtained may corroborate that TeNPs were internalized by the bacterial cells or attached to bacteria cell wall.

After the disruption of the cell walls, the intensity of the events produced by individual nanoparticles was lower than those related to intact cells that could have accumulated more than one TeNP. With the knowledge of the mass of an individual particle and the mass of Te accumulated per cell from previous sections, the number of TeNPs internalized or associated to bacterial cell wall was calculated. Table 3 displays the average of nanoparticles detected in individual bacterial cells as well as the minimum and maximum number of particles after exposure to the three different Te

concentrations. The number of particles increased with the applied TeNPs concentrations. Cells containing one single TeNP only appear at 0.5 mg Te L-1 whereas cells containing multiple TeNPs were detected at the higher concentrations in both bacterial strains.

No significant differences between strains regarding to the number of particles accumulated were observed, although the maximum number of particles was higher in E. coli, probably due to the increased cell size.

3.4 Sizing rod-shaped TeNPs by SP-ICP-MS and TEM measurements

Finally, the dimensional characterization of tellurium nanorods formed through the interaction of bacteria with the original spherical TeNPs was explored. Single-particle ICP-MS is a valuable technique that enables the mass determination of individual particles. Provided that the particles are of spherical shape, it is well established to convert the mass of the particle into its size [42]. However, characterization of non-spherical nanoparticles by employing SP-ICP-MS is still in its infancy [43].

In the current work, dimensional size characterization of rod-shaped tellurium nanoparticles has been performed by employing TEM and SP-ICP-MS analysis. It is important to highlight that the calculations for estimating the width and length of tellurium nanorods have been carried out by considering these nanoparticles with a cylindrical morphology. The procedure developed consisted on a step-by-step approach: 1) determination of the volume of nanorods by particle mass data (SP-ICP-TQ-MS) and particle density (from nanorods composition provided by X-ray diffraction, considering 99 % TeO_2 and 1 % Te) and 2) estimation of width and length of tellurium nanorods by employing the formula for the volume of a cylinder and the aspect ratio previously determined by TEM analysis. The particle size detection limit for SP-ICP-MS was calculated by using the approach of Abad-Alvaro et al [44] and by applying the 3σ criterion. Based on that , the LOD size was 28 nm. Therefore, those particles with a

volume below 11,494 nm3 were not considered for tellurium nanorods dimensional estimations. Consequently, and by assuming a LOD size of 28 nm, the smallest volumes employed for calculations were about 12,505 nm^3 and 15,492 nm^3 for *E. coli* and *S. aureus* experiments, respectively and corresponding to a minimum width of around 11 and 12 nm. A similar procedure has been reported by Kalomista *et al.* for dimensional size characterization of rod-shaped gold nanoparticles [43].

Figures 6 and 7 show width and length size histograms calculated from tellurium nanorods isolated from *E. coli and S. aureus*, respectively, after exposure to the different Te concentrations. The histogram profiles clearly demonstrate the variability of the nanorods dimensions, which confirms the heterogeneity of bacterial cell behaviour concerning the morphological TeNPs transformations and uptake. Furthermore, mean values for width and length calculated with SP-ICP-MS agreed well with those values provided by TEM at the highest concentration of TeNPs tested. No TEM data were available for comparison at the low exposition levels, since this technique was unable to detect the nanorods under those conditions. However, the SP-ICP-MS strategy developed here, is capable of providing data on the size of the nanorods at the lowest levels of exposure (0.5 and 1 mg Te L^{-1}), confirming that these are similar in width, but shorter in length than the ones produced after exposure to 15 mg Te L^{-1} in both species of bacteria.

4. Conclusions

This study shows for the first time the application of SC-ICP-TQ-MS for quantifying the uptake and distribution of TeNPs at single cell level in Gram-positive and Gram-negative bacteria model organisms, *S. aureus* and *E. coli*, respectively. Moreover, the combination of flow cytometry (bacterial cell population) and ICP-TQ-MS (phosphorous content) has enable to track cell transport until the plasma, achieving under optimal conditions, cell introduction efficiencies as high as (74 ± 6) % and (85 ± 7) % for *E. coli* and *S. aureus*, respectively. The results obtained confirmed the existence of a great

cell to cell variability in terms of TeNPs uptake and number of particles accumulated. TEM analysis together with X-ray diffraction measurements evidenced compositional and morphological changes of TeNPs from nanospheres to nanorods as a consequence of bacteria-nanoparticle interaction. The combination of SP-ICP-MS and TEM has allowed us to estimate the dimensions of nanorods produced by both bacterial strains. The values obtained agreed well with the values calculated from TEM images confirming the feasibility of the proposed strategy for the dimensional characterization of non-spherical nanoparticles and overcoming size limitations for TEM detection.

Author contributions

All authors have given approval to the final version of the manuscript.

Notes

The authors declare no competing financial interest.

Acknowledgements

The authors gratefully acknowledge the financial support from Spanish Ministry for Science, Innovation and Universities (CTQ2017-83569-C2-1-R, RTI2018-094605-B-I00, FC-GRUPIN-IDI/2018/000242), the Community of Madrid and European funding from FSE and FEDER programs (project S2018/BAA-4393, AVANSECAL-II CM), as well as the support from the Asturian Foundation for Biosanitary Research and Innovation (FINBA). Thermo Fisher Scientific, Bremen, Germany, and Teledyne Cetac Technologies, Omaha, NE, USA, are acknowledged for their instrumental support.

Supporting Information.

Table S1: Operating parameters of the ICP-TQ-MS system for the single cell and single cell experiments. Table S2: Percentage of viable and non-viable cell after the exposure of *S.aureus* and *E.coli* to TeNPs obtained from flow cytometry analysis (mean ± SD; n=3). Figure S1:TEM images and EDXS spectrum of TeNPs dispersed

(a) in water and (b) in LB medium. (c) X-ray diffraction pattern of TeNPs. Figure S2: TEM images of a thin section of fixed E. coli (a) and S.aureus (b) treated with (0.5 mg Te L^{-1} as TeNPs. Figure S3:Time resolved SC-ICP-MS analysis of $^{31}P^{16}O+$ for S. aureus cells treated with (a) 0, (b) 0.5, (c) 1, and (d) 15 mg Te L-1 as TeNPs. Figure S4. Time resolve SC-ICP-MS analysis of ^{31} P16O+ for E, coli treated with with (a) 0, (b) 0.5, (c) 1, and (d) 15 mg Te L-1 as TeNPs.

Figures Captions

Figure 1: TEM images, EDXS spectra and concentring ring (a, b) and X-ray diffraction pattern (c, d) of rod-shaped TeNPs found in (a, c) *S. aureus* and (b, d) *E. coli* experiments.

Figure 2: TEM images of a thin section of fixed E. coli treated with (a) 0, (b) 1, and (c and d) 15 mg Te L^{-1} as TeNPs and *S. aureus treated* with (e) 0, (f) 1.0, and (g and h) 15 mg Te L^{-1} as TeNPs. Red arrows indicate morphological changes in bacteria and white arrows rod-shaped TeNPs.

Figure 3: Time resolved SC-ICP-MS analyses of (a-d) ^{126}Te and the corresponding frequency histograms (e-g) for *S. aureus* cells treated with (a) 0, (b) 0.5, (c) 1, and (d) 15 mg Te L^{-1} as TeNPs.

Figure 4: Time resolved SC-ICP-MS analyses of (a-d) ^{126}Te and the corresponding frequency histograms (e-g) for *E. coli* cells treated with (a) 0, (b) 0.5, (c) 1, and (d) 15 mg Te L^{-1} as TeNPs.

Figure 5: Time resolved SC/SP-ICP-MS analyses of ^{126}Te before (a and c) and after bacterial wall disruption (b and d) of *E. coli* (a and b) and *S. aureus* (c and d) cells treated with 15 mg Te L^{-1} as TeNPs.

Figure 6: Size distribution histogram obtained from SP-ICP-MS analysis for width and length dimensions of rod-shaped TeNPs isolated from *E. coli* cells treated with (a and b) 0.5, (c and d) 1 and (e and f) 15 mg Te L^{-1} as TeNPs.

Figure 7: Size distribution histogram obtained from SP-ICP-MS analysis for width and length dimensions of rod-shaped TeNPs isolated from *S. aureus* cells treated with (a and b) 0.5, (c and d) 1 and (e and f) 15 mg Te L^{-1} as TeNPs.

Tables.

Table 1: Percentage of Te accumulated in *S.aureus* and *E. coli* after their exposure to different concentration of TeNPs (mean ± SD; n=3).

	S.aureus	*E.coli*
[TeNPs] mg Te L^{-1}	% Te	% Te
0.5	97 ± 3	48 ± 3
1	100 ± 10	38 ± 1
15	105 ± 9	28 ± 4

Table 2: Te levels in *S. aureus* and *E .coli* after incubation with 0.5, 1, 15 mg Te L^{-1} as TeNPs by SC-ICP-MS and after acid digestion (mean ± SD; n=3).

	S. aureus		*E. coli*	
[TeNPs] mg Te L^{-1}	SC-ICP-MS fg cell $^{-1}$	Digestion /ICP-MS fg cell $^{-1}$	SC-ICP-MS fg cell $^{-1}$	Digestion /ICP-MS fg cell^{-1}
0.5	0.77 ± 0.22	0.79 ± 0.12	0.30 ± 0.13	0.24 ± 0.10
1	1.20 ± 0.53	1.10 ± 0.22	0.44 ± 0.21	0.47 ± 0.21
15	12.80 ± 5.58	18.19 ± 2.34	12.43 ± 4.36	14.96 ± 2.52

Table 3: Average of TeNPs internalized or associated to bacteria cell wall per *S. aureus* and *E. coli* individual cell after the incubation of both strains with 0.5, 1, 15 mg Te L^{-1} as TeNPs determined by SP-ICP-MS after bacterial cell lysis.

[TeNPs]	*S.aureus*			*E.coli*		
mg Te L^{-1}	TeNPs $cell^{-1}$			TeNPs $cell^{-1}$		
	Min	Max	Mean	Min	Max	Mean
0.5	1	9	5 ± 2	1	4	4 ± 1
1	2	13	9 ± 4	2	11	7 ± 3
15	3	95	37 ± 27	3	122	50 ± 36

References

[1] Nasrollahzadeh, M.; Sajadi, S.M.; Sajjadi, M.; Issaabadi, Z. Application of nanotechnology in daily life. *Interf. Sci. Technol.* **2019**, 28, 113-143.

[2] Katz, L.M.; Dewan, K.; Bronaugh, R.L. Nanotechnology in cosmetics. *Food Chem. Toxicol .* **2015**, 85, 127- 137.

[3] Gupta, R.; Xie, H. Nanoparticles in daily life: Applications, Toxicity and Regulations. *J. Environ. Pathol. Toxicol. Oncol.* **2018**, 37(3), 209-230.

[4] Pathakoti, K.; Manubolu, M.; Hwang, H.M. Nanostructures current uses and future applications in food science. *J. Food Drug Anal.* **2017**, 25, 245-253.

[5] Zheng, K.; Setyawati, M.I.; Leong, F.T.; Xie, J. Antimicrobial silver nanomaterials. *Coord. Chem. Rev.* **2018**, 357, 1-17.

[6] Lead, J.R.; Batley, G.E.; Alvarez, P.J.J.; Croteau, M.N.; Handy, R.D.; McLaughlin, M.J.; Judy, J.D.; Schrimer, K. Nanomaterials in the environment: behavior, fate, bioavailability, and effects-an updated review. *Environ. Toxicol. Chem.* **2018**, 37, 2029-2063.

[7] Kruszewska, J.; Kur, A., Kulpinska, D.; Grabowska-Jadach, I.; Matczuk, M.; Keppler, B.K.; Timerbaev, A.R.; Jarosz, M. An improved protocol for ICP-MS based assessment of the celular uptake of metal-based nanoparticles. *J. Pharm. Biomed. Anal.* **2019**, 174, 300-304.

[8] Matczuk, M.; Ruzik, L.; Alksenko, S.S.; Keppler, B.K.; Jarosz, M.; Timerbaev, A.R. Analytical methodology for studying cellular uptake, processing and localization of gold nanoparticles. *Anal. Chim. Acta* **2019**, 1052, 1-9.

[9] Wei, X.; Dong-Hua, Z.; Cai, Y.; Jiang, R.; Chen, M.L.; Yang, T.; Xu, Z.R.; Yu, Y.L.; Wang, J.H. High-Throughput/High-Precision sampling of single cells into ICP-MS for elucidating cellular nanoparticles. *Anal. Chem.* **2018**, 90, 14543-14550.

[10] Merrifield, R. C.; Stephan, C.; Lead, J. Determining the concentration dependent transformations of Ag nanoparticles in complex media: Using SP-ICP-MS and Au@Ag core shell nanoparticles as tracers. *Environ. Sci. Technol.* **2017**, 51, 3206−3213.

[11] Loeschner, K.; Navratilova, J.; Kobler, C.; Molhave, K.; Wagner, S.; von der Kammer, F.; Larsen, E.H. Detection and characterization of silver nanoparticles in chicken meat by asymmetric flow field flow fractionation with Detection by conventional or single particle ICP-MS. *Anal. Bioanal. Chem.* **2013**, 405, 8185-8195.

[12] Loeschner, K.; Brabrand, M.S.J.; Sloth, J.J.; Larsen, E.H. Use of alkaline or enzymatic sample pretreatment prior to characterization of gold nanoparticles in animal tissue by single-particle ICPMS. *Anal. Bioanal. Chem.* **2014**, 406, 3845-3851.

[13] Peters, R.J.; Rivera, Z.H.; Van Bemmel, G.; Marvin, H.J.; Weigel, S.; Bouwmeester, H. Development and validation of single particle ICP-MS for sizing and quantitative determination of nano-silver in chicken meat. *Anal. Bioanal. Chem.* **2014**, 406, 3875-3885.

[14] Dan, Y.; Zhang, W.; Xue, R.; Ma, X.; Stephan, C.; Shi, H. Characterization of gold nanoparticle uptake by tomato plants using enzymatic extraction followed by single-particle inductively coupled plasma-mass spectrometry analysis. *Environ. Sci. Technol.* **2015**, 49, 3007-3014.

[15] Laborda, F.; Bolea, E.; Jimenez-Lamana, J. Single particle inductively coupled plasma mass spectrometry for the analysis of inorganic engineered nanoparticles in environmental samples. *Trends Environ. Anal. Chem.* **2016**, 9, 15-23.

[16] Li, F.; Armstrong, D. W.; Houk, R. S. Behavior of bacteria in the inductively coupled plasma: Atomization and production of atomic ions for mass spectrometry. *Anal. Chem.* **2005**, 77, 1407-1413.

[17] Wang, H.; Wang, M.; Wang, B.; Zheng, L.; Chen, H.; Chai, Z.; Feng, W. Interrogating the variation of element masses and distribution patterns in single cells using ICP-MS with a high efficiency cell introduction system. *Anal. Bioanal. Chem.* **2017**, 409, 1415-1423.

[18] Shigeta, K.; Koellensperger, G.; Rampler, E.; Traub, H.; Rottmann, L.; Panne, U.; Okinoc, A.; Jakubowski, N. Sample introduction of single selenized yeast cells (Saccharomyces cerevisiae) by micro droplet generation into an ICP-sector field mass spectrometer for label-free detection of trace elements. *J. Anal. At. Spectrom.* **2013**, 28:637-645.

[19] Corte, M.; Alvarez-Fernández, R.; Blanco, E.; Bettmer, J.; Montes-Bayón, M. Quantitative evaluation of cisplatin uptake in sensitive and resistant individual cells by single-cell ICP- MS (SC-ICP-MS). *Anal. Chem.* **2017**, 89, 11491-11497.

[20] Wang, H.; Chen, B.; He, M.; Hu, B. A facile Droplet-Chip-Time-Resolved Inductivvely Coupled Plasma Mass Spectrometry Online System for determination of zinc in single cell. *Anal. Chem.* **2017**, 89(9), 4931-938

[21] Lopez-Serrano, A.; Baumgart, S.; Bremser, W.; Fleming, S.; Wittke, D.; Grützkau, A.; Luch, A.; Haase, A.; Jaubowski, N. Quantification of silver nanoparticles up-taken by single cell using inductively coupled plasma mass spectrometry in the single cell measurement mode. *J. Anal. At. Spectrom.* **2018**, 33, 1256-1263.

[22] Mavrakis, E.; Mavroudakis, L.; Lydakis-Simantiris, N.; Pergantis, SA. Investigating the uptake of arsenate by Chlamydomonas reinhardtii cells and its effect of their lipid profile using single cell ICP-MS and easy ambient sonic-spray ionization-MS. *Anal. Chem.* **2019**, 91, 9590-9598.

[23] Álvarez-Fernández García, R.; Corte-Rodríguez, M.; Macke, M.; LeBlanc, K.; Mester, Z.; Montes-Bayon, M.; Bettmer, J. Addressing the Presence of Biogenic Selenium Nanoparticles in Yeast Cells: Analytical Strategies Based on ICP-TQ-MS. *Analyst* **2020**, DOI: 10.1039/C9AN01565E.

[24] Merrifield, R.C.; Stephan, C.; Lead, J.R. Quantification of Au nanoparticles biouptake and distribution to freshwater algae using single cell ICP-MS. *Environ. Sci. Technol.* **2018**, 52, 2271-2277.

[25] Feng, Z.V.; Gunsolus, I.L.; Qiu, T.A.; Hurley, K.R.; Nyberg, L.H.; Frew, H.; Johnson, K.P.; Varanian, A.; Jacob, L.M.; Lohset, S.E.; Torelli, M.D.; Hamers, R.J.;

Murphy, C.J.; Haynes, C.L. Impact of gold nanoparticle charge and ligand type on surface binding and toxicity to Gram-negative and Gram-positive bacteria. *Chem. Sci.* **2015**, 6, 5186-5196.

[26] Nguyen, V.K.; Choi, W.; Ha, Y.; Gu, Y.; Lee, C.; Park, J.; Jang, G.; Shin, C.; Cho, S. Microbial tellurite reduction and production of elemental tellurium nanoparticles by novel bacteria isolated from wastewater. *J. Ind. Eng. Chem.* **2019**, 78, 246-256.

[27] Mousavi-Kamazani, M.; Rahmatolahzadeh, R.; Shobeiri, S.A.; Beshkar, F. Sonochemical synthesis, formation mechanism, and solar cell application of tellurium nanoparticles. *Ultrason. Sonochem*. **2017**, 39, 233-239.

[28] Ba, L.A.; Doring, M.; Jamier, V.; Jacob, C. Tellurium: an element with great biological potency and potential. *Org. Biomol. Chem*., **2012**, 8(19), 4203-16.

[29] Figueroa, M.; Fernandez, V.; Arenas-Salinas, M.; Ahumada, D.; Muñoz-Villagrán, C.; Cornejo, F.; Vargas, E.; Latorre, M.; Morales, E.; Vásquez, C.; Arenas, F. Synthesis and antibacterial activity of metal(loid) nanostructures by environmental multi-metal(loid) resistant bacteria and metal(loid)-reducing flavoproteins. *Front.Microbiol*. **2018,** 15 (9), 959.

[30] Huang, W.; Wu, H.; Li, X.; Chen, T. Facile one-pot synthesis of tellurium nanorods as antioxidant and anticancer agents. *Chem. Asian. J.* **2016**, 11(16), 2301-11.

[31] Medina, D.; Tien-Streen, W.; Zhang, B.; Huang, X.; Vernet, A.; Nieto-Argüello, A.; Cholula-Díaz, J.L.; Martínez, L.; Huttel, Y.; Ijué, M.; García-Martín, J.M.; Webster, T.J. Citric juice-mediated synthesis of tellurium nanoparticles with antimicrobial and anticancer properties. *Green Chem.,* **2019**, 21, 1982-1998.

[32] Shakibaie, M.; Adeli-Sardou, M.; Mohammadi-Khorsand, T.; Zeydabadi-Nejad, M.; Amirafzali, E.; Amirpour-Rostami, S.; Ameri, A.; Forootanfar, H. Antimicrobial and antioxidant activity of the biologically synthesized tellurium nanorods; a preliminary In vitro study. *Irani J. Biotech.*, **2017**, 15(4), 268-276.

[33] Gómez-Gómez, B.; Arregui, L.; Serrano, S.; Santos, A.; Pérez-Corona, t.; Madrid, Y. Selenium and tellurium-based nanoparticles as interfering factors on Quorum

sensing-regulated processes: violacein production and bacterial biofilm formation. *Metallomics* **2019**, 11, 1104-1114.

[34] Gómez-Gómez, B.; Sanz-Landaluze, J.; Pérez-Corona, M.T.; Madrid, Y. Fate and effect of in-house synthesized tellurium based nanoparticles on bacterial biofilm biomass and architecture. Challenges for nanoparticles characterization in living systems. *Sci. Total Environ*. **2020**, 719, 137501.

[35] Corte-Rodríguez, M.; Blanco-González, E.; Bettmer, J.; Montes-Bayón, M. Quantitative Analysis of Transferrin Receptor 1 (TfR1) in Individual Breast Cancer Cells by Means of Labeled Antibodies and Elemental (ICP-MS) Detection. *Anal. Chem.* **91**, 15532-15538.

[36] Borguese, B.; Brucale, M.; Fortunato, G.; Lanzi, M.; Mezzi, A.; Valle, F., Cavallini, M.; Zannoni, D. Extracellular production of tellurium nanoparticles by the photosyntetic bacterium Rhodobacter capsulatus. *J. Hazard. Mater.* **2016**, 309, 202-209.

[37] Zare, B.; Faramarzi, M.A.; Sepehrizadeh, Z.; Shakibaie, M.; Rezaie, S.; Shahverdi, A.R. Biosynthesis and recovery of rod-shaped tellurium nanoparticles and their bactericidal activities. *Mater. Res. Bull.* **2012**, 47, 3719-3725.

[38] Shakibaie, M.; Adeli-Sardou, M.; Mohammadi-Khorsand, T.; Zeydabadi-Nejad, M.; Amirafzali, E.; Amirpour-Rostami, S.; Ameri, A.; Forootanfar, H. Antimicrobial and antioxidant activity of the biologically synthesized tellurium nanorods; a preliminary In vitro Study. *Iran. J. Biotechnol.* **2017**, 15, e1580.

[39] Vaigankar, D.C.; Dubey, S.K.; Mujawar, S.Y.; d´Costa, A.; Shyama, S.K. Tellurite biotransformation and detoxification by Shewanella baltica with simultaneous synthesis of tellurium nanorods exhibiting photo-catalytic and anti-biofilm activity. *Ecotox. Environ. Safe.* **2018**, 165, 516-526.

[40] Kim, D.H.; Kanaly, R.A.; Hur, H.G. Biological accumulation of tellurium nanorod structures via reduction of tellurite by Shewanella oneidensis MR-1. *Bioressour. Technol.* **2012**, 125, 127-131.

[41] Doherty, G.J.; McMahon, H.T. Mechanisms of endocytosis. *Ann. Rev. Biochem.* **2009**, 78, 857-902.

[42] Laborda, F.; Bolea, E.; Jiménez-Lamana, J. Single Particle Inductively Coupled Mass Spectrometry: A powerful tool for nanoanalysis. *Anal. Chem.* **2014**, 86, 2270-2278.

[43] Kalomista, I.; Keri, A.; Unqor, D.; Csapó, E.; Dékány, I.; Prohaska, T.; Galbács, G. Dimensional characterization of gold nanorods by combining millisecond and microsecond temporal resolution single particle ICP-MS measurements. *J. Anal. At. Spectrom*. **2017**, 32, 2455-2462.

[44] Abad-Álvaro, I.; Peña-Vázquez, E.; Bolea, E.; Bermejo-Barrera, P.; Castillo, J.R.; Laborda, F. Evaluation of Number concentration quantification by single particle inductively coupled plasma mass spectrometry microsecond vs millisecond dwell times, *Anal. Bioanal. Chem*. **2016**, 408, 5089-5097.

Figure 1.

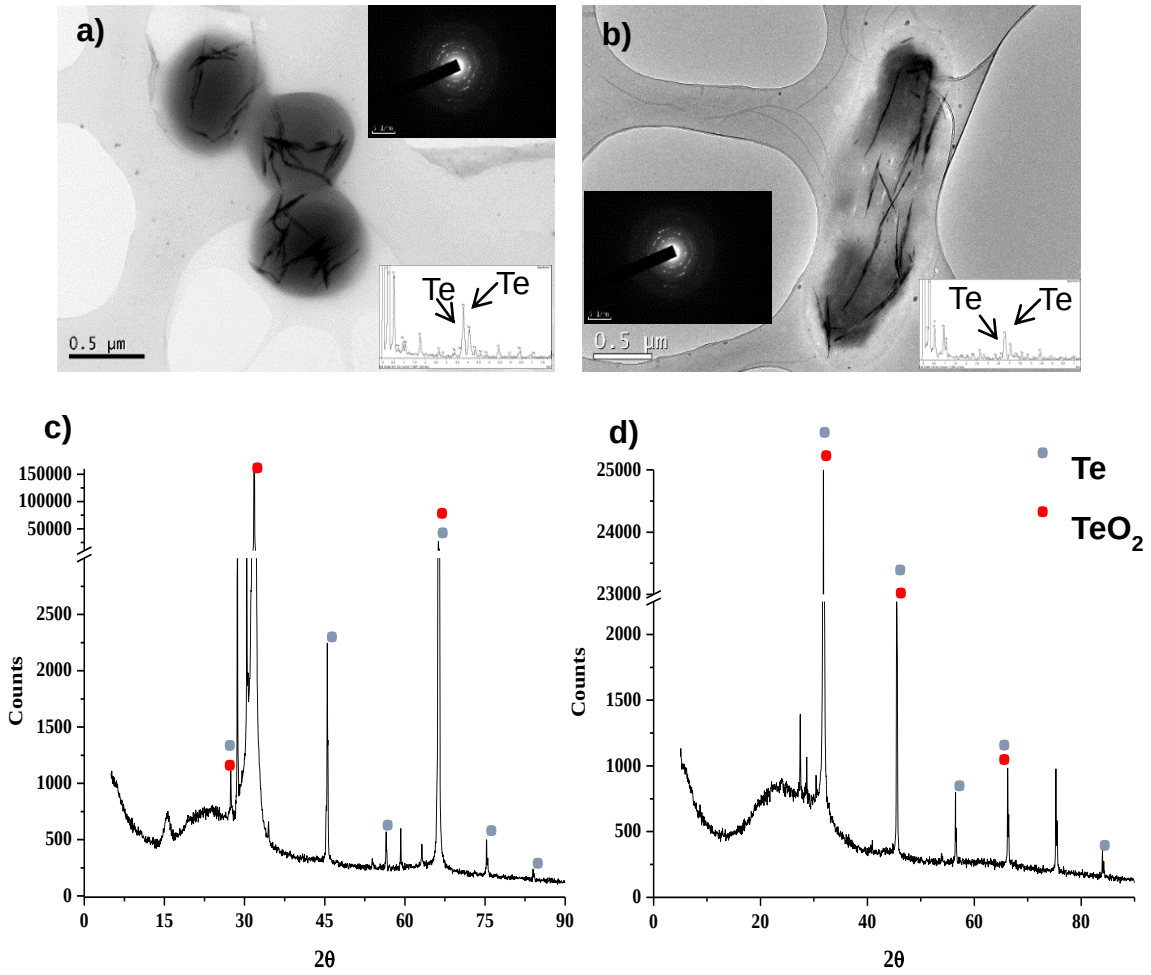

Figure 2.

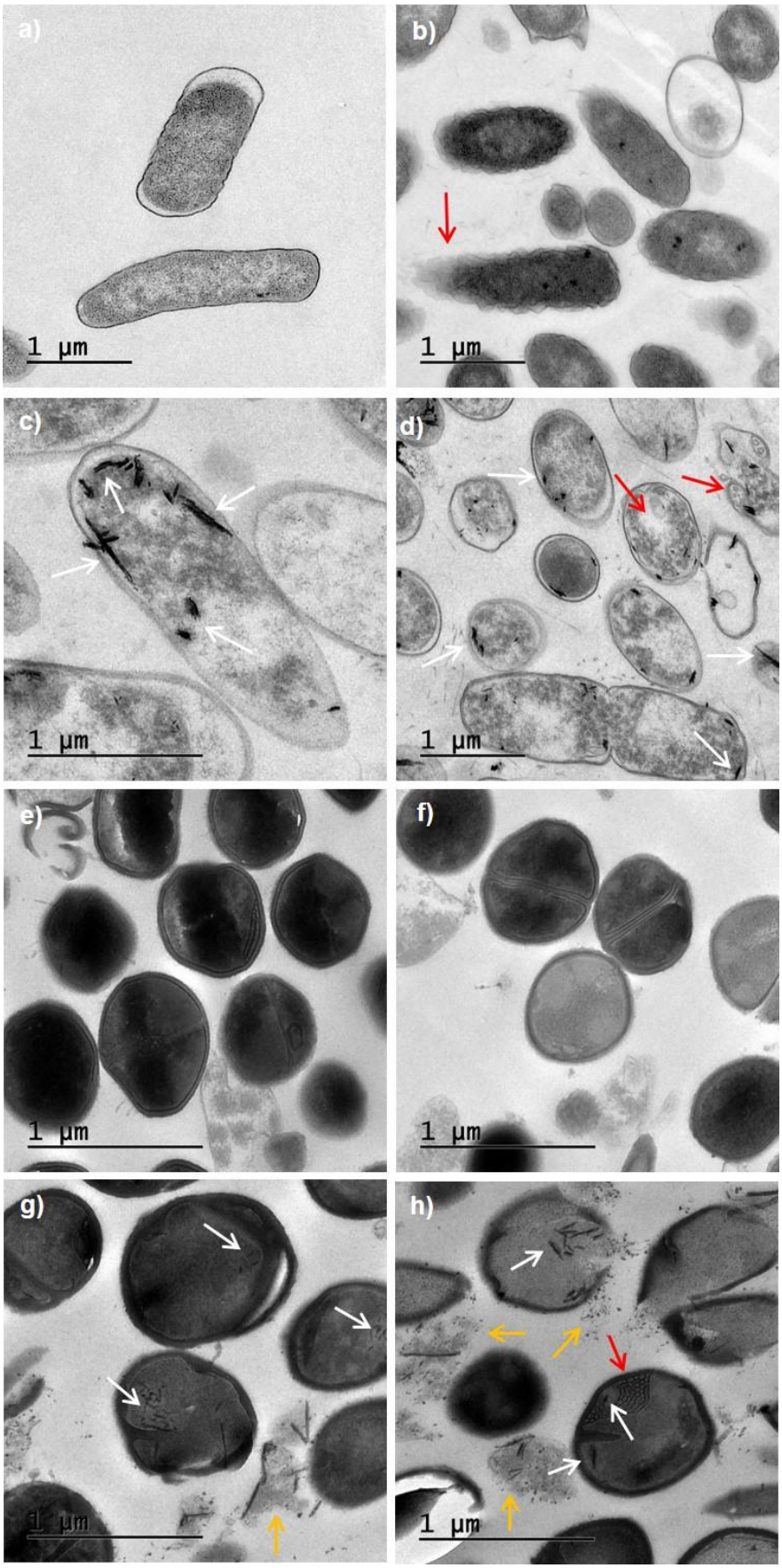

Figure 3.

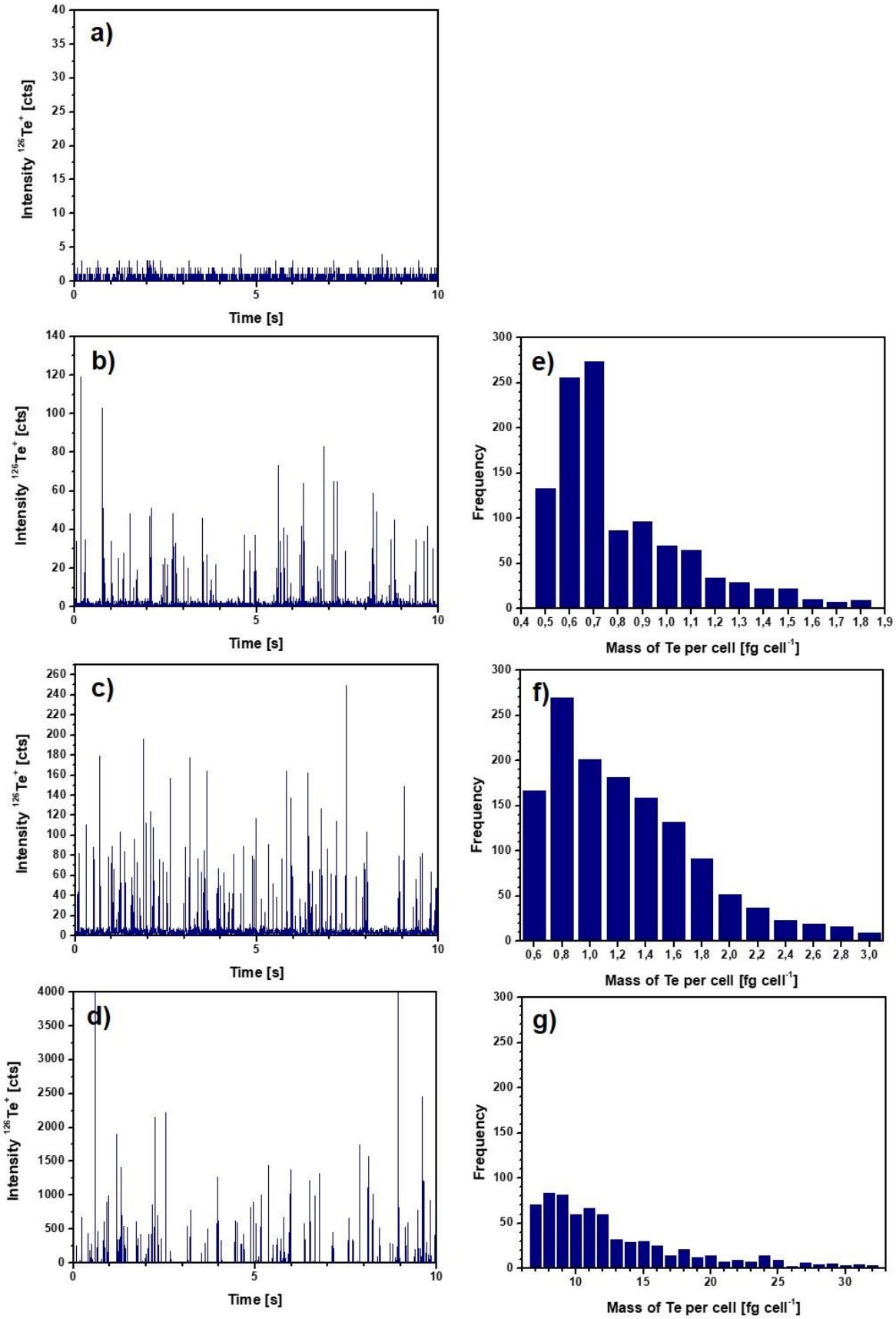
a)
b)
c)
d)
e)
f)
g)
Intensity $^{126}Te^+$ [cts]
Time [s]
Frequency
Mass of Te per cell [fg cell^{-1}]

Figure 4.

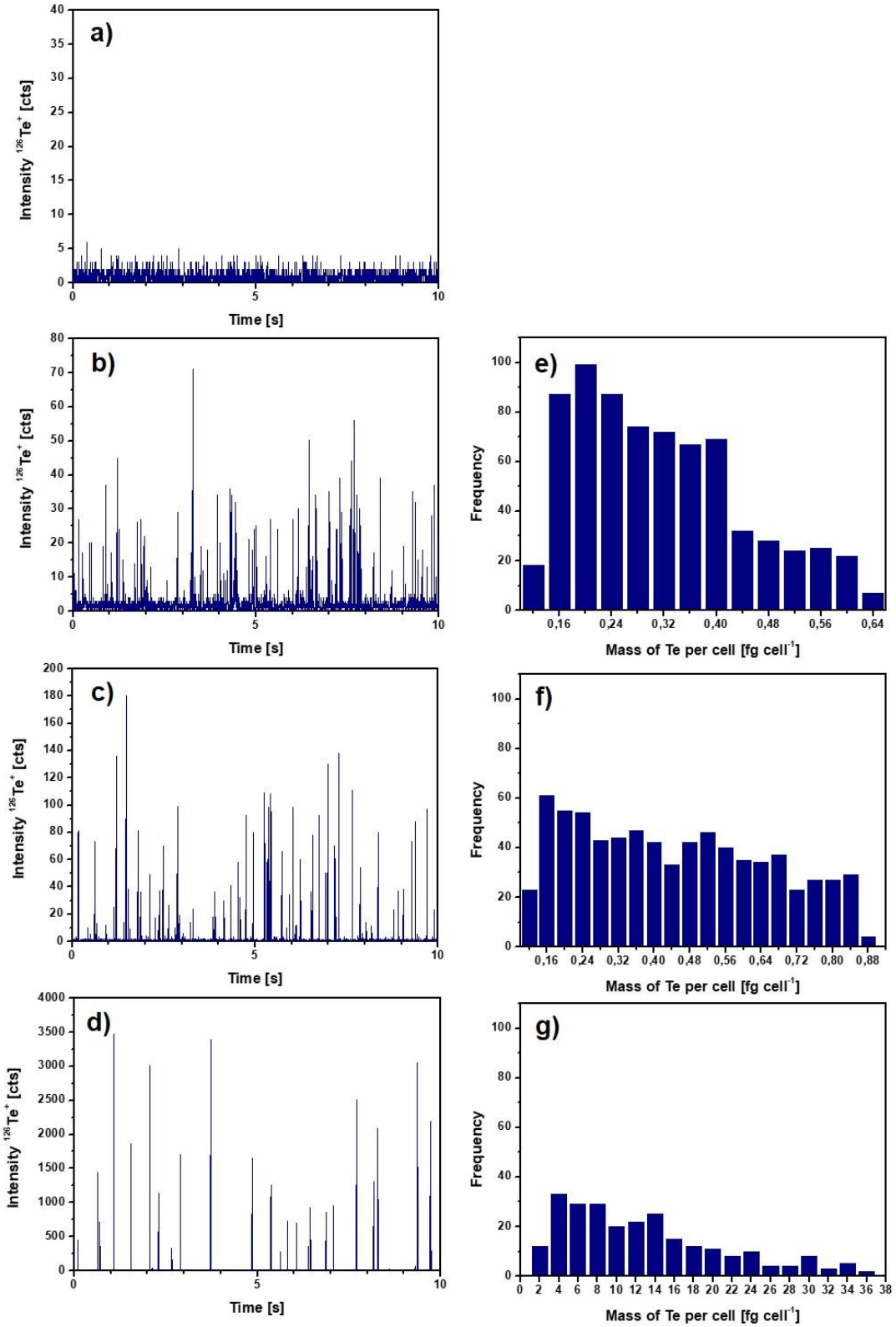
a)
b)
c)
d)
e)
f)
g)
Intensity $^{126}Te^+$ [cts]
Time [s]
Frequency
Mass of Te per cell [fg cell^{-1}]

Figure 5.

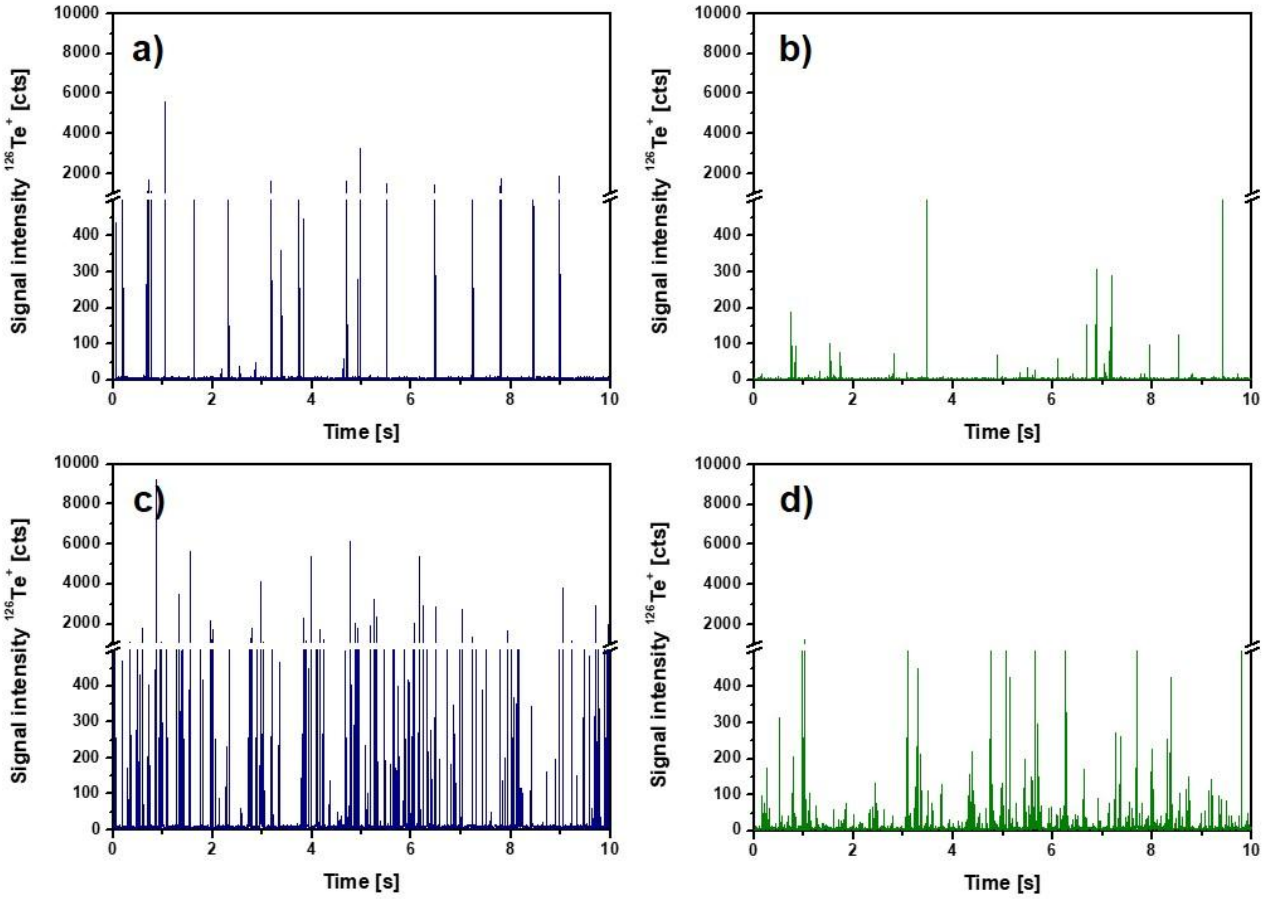
a)
b)
c)
d)
Signal intensity $^{126}Te^{+}$ [cts]
Time [s]
10000
8000
6000
4000
2000
400
300
200
100
0
0
2
4
6
8
10

Figure 6.

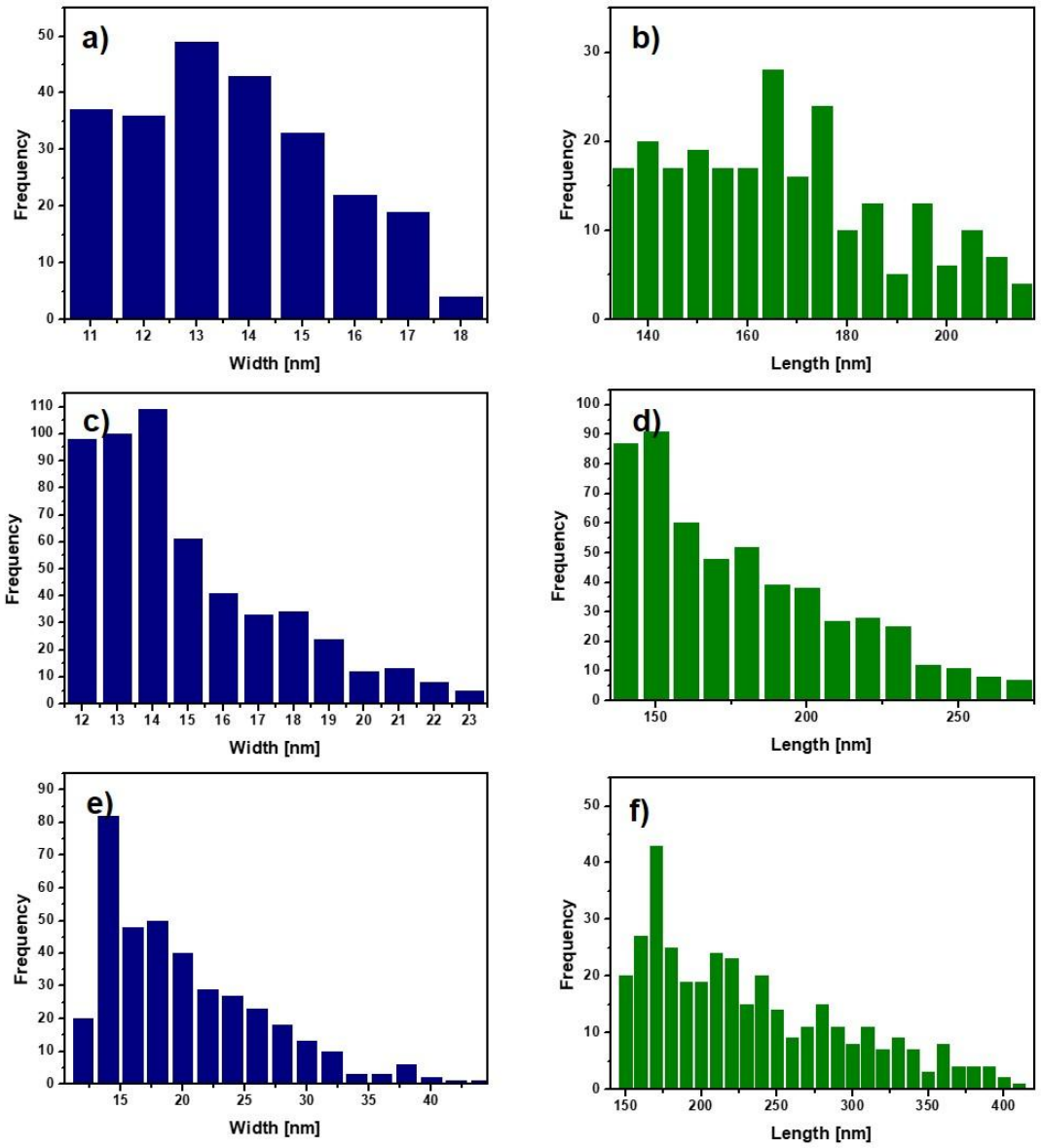
a)
Frequency
Width [nm]
b)
Frequency
Length [nm]
c)
Frequency
Width [nm]
d)
Frequency
Length [nm]
e)
Frequency
Width [nm]
f)
Frequency
Length [nm]

Figure 7.

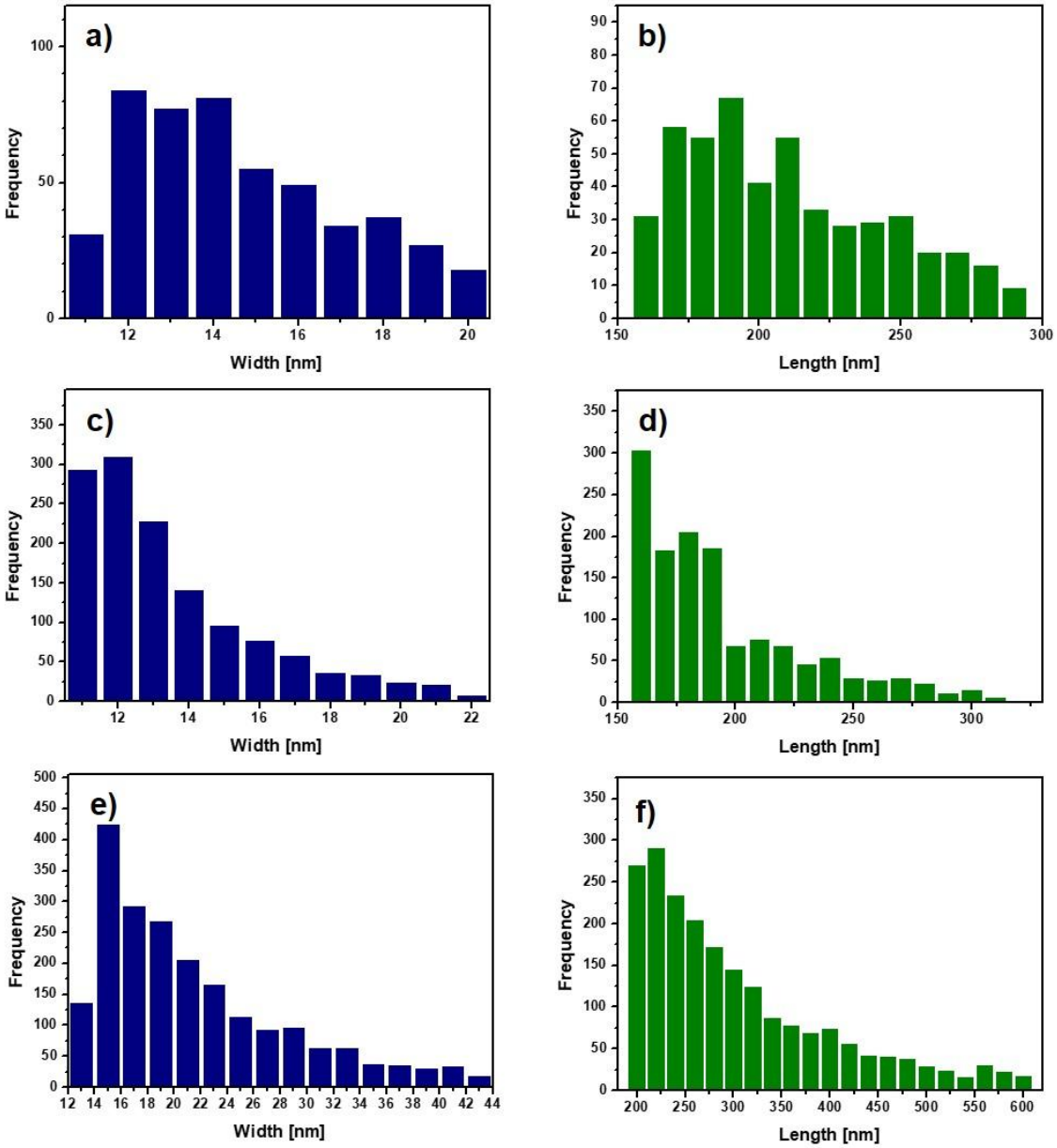
a)
Frequency
Width [nm]
b)
Frequency
Length [nm]
c)
Frequency
Width [nm]
d)
Frequency
Length [nm]
e)
Frequency
Width [nm]
f)
Frequency
Length [nm]